HHS Public Access

Author manuscript

Biochemistry. Author manuscript; available in PMC 2017 October 19.

Published in final edited form as:

Biochemistry. 2017 June 13; 56(23): 2950–2966. doi:10.1021/acs.biochem.6b01187.

Remote Perturbations in Tertiary Contacts Trigger Lysine Ligation to the Heme Iron in Cytochrome *c*

Jie Gu[†], **Dong-Woo Shin**[†], and **Ekaterina V. Pletneva**[*]

Department of Chemistry, Dartmouth College, Hanover, NH 03755

Abstract

Perturbations in protein structure define the mechanism of allosteric regulation and biological information transfer. In cytochrome *c* (cyt *c*), Met80 ligation to the heme iron is critical for the protein's electron-transfer (ET) function in oxidative phosphorylation and for suppressing its peroxidase activity in apoptosis. The hard base Lys is a better match for the hard ferric iron than the soft base Met, suggesting the key role of the protein scaffold in favoring Met ligation. To probe the role of the protein structure in maintenance of Met ligation, mutations T49V and Y67R/M80A were designed to disrupt hydrogen bonding and packing of the heme coordination loop, respectively. Electronic absorption, NMR, and EPR spectra reveal that ferric forms of both variants are Lys-ligated at neutral pH. A minor change in the tertiary contacts in T49V, away from the heme coordination loop, appears to be sufficient to execute a change in ligation, suggesting a cross-talk between the different regions of the protein structure and a possibility of built-in conformational switches in cyt *c*. Analyses of thermodynamic stability, kinetics of Lys binding and dissociation and the pH-dependent changes in ligation provide detailed characterization of the Lys coordination in these variants and relate these properties to the extent of structural perturbations. The findings emphasize the importance of the hydrogen-bonding network in controlling the native Met80 ligation to the heme iron.

TOC image

[*]Corresponding author: ekaterina.pletneva@dartmouth.edu, Tel. 1-603-646-0933, Fax: 1-603-646-3946.
[†]The authors have contributed equally to this work

Supporting Information Available. One table showing pK_a values for the alkaline transition in previously studied variants; twelve figures showing 2D ^{1}H NMR spectra of ferrous WT, T49V, and T49V Met-SO; NMR, EPR, and UV-visible spectra of ferric M80A at different pH values; visible CD spectra of the studied variants; comparison of the ^{1}H NMR spectra of ferrous K73A/K79G/M80K, Y67R/M80A, and M80A; the downfield region of the ^{1}H NMR spectra of the studied ferric variants at pD 4.5; NMR and EPR spectra of studied ferric variants at alkaline pH; pH-dependent EPR and NMR spectra of T49V; pH-dependent EPR and NMR spectra of Y67R/M80A; pH-dependent visible spectra (CT) region of T49V; pH-dependent visible spectra (CT) region of Y67R/M80A; input-independent component spectra from SVD analysis of T49V; representative kinetic traces from pH-jump and imidazole-binding experiments.

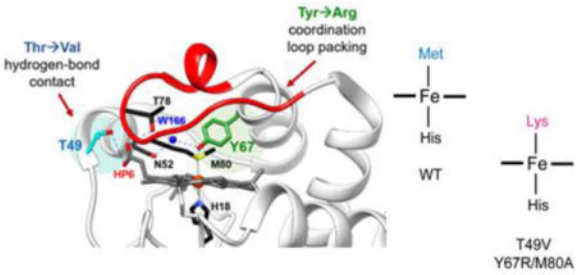

Perturbations of protein structure and dynamics define the mechanisms of allosteric regulation and biological information transfer. The extent of such perturbations ultimately depends on the properties of the protein folding landscape.[1] By analyzing these changes, one can learn about the critical interactions that define the native protein fold and identify the built-in switches to alternatively-folded forms that have profound implications for function.

The mitochondrial heme protein cytochrome *c* (cyt *c*) is an excellent system for studies of conformational switching. Several conformational forms of cyt *c*, some induced by biologically-relevant triggers[2] and others populated under denaturing conditions,[3–5] have been identified by spectroscopic studies. At neutral pH the protein is in its compact globular form, with the ligands His18 and Met80 coordinated to the heme iron (Figure 1).[6] This conformation is associated with the function of cyt *c* as an electron carrier in oxidative phosphorylation. Binding of cyt *c* to cardiolipin (CL)-rich membranes promotes changes in the heme iron ligation and tertiary structure of the protein that activate it for peroxidase function, which is critical in early stages of apoptosis.[7,8] The native Met80 coordination to the heme is lost upon CL binding and other strong endogenous ligands take its place in the observed low-spin heme iron species. Both compact and extended CL-bound species of cyt *c* have been observed; their partitioning depends on a number of factors, including the CL content of the membrane and the available surface area.[9]

Residues His and Lys have been suggested to act as heme iron ligands in the CL-bound cyt *c*, with the former being more likely the ligand in the largely unfolded extended CL-bound species.[10] In equine protein, His26 and His33 coordinate to the heme iron under denaturing conditions at neutral pH, and these misligated species behave as kinetic traps, slowing down the protein folding.[11] Similarly, misligated species with Lys at the heme iron have been observed in urea-denatured cyt c^4 and have been proposed to form upon binding of the protein to CL.[12] Lys is also a heme iron ligand in cyt *c* at high solution pH and this conformational form, known as the alkaline state, has been the subject of intense research.[13–17] In addition to its relevance to the CL-bound compact species, the alkaline form has been suggested to play a regulatory role in physiological electron transfer (ET)[18] and to be useful as a model for late folding intermediates.[19]

Careful studies have shown that Lys73 or Lys79 within the heme coordination loop (Ω-loop D, residues 70–85) coordinate to the heme iron at alkaline pH.[14] The NMR structure of Lys73-ligated cyt *c* at pH 11.1 has shown that most of the native protein core is maintained in this conformational form, but the heme coordination loop is largely unstructured and there are changes in the positions of other Ω-loops.[20] Thermodynamic studies of ligand binding to

the model heme peptide microperoxidase-8 (MP8) have illustrated that the hard base Lys is a better match for the hard ferric iron, compared to the soft base Met.[21,22] Deprotonation of the Lys sidechain (pK_a>10), as well as destabilization of the heme coordination loop, favor the Lys ligation at this high pH.

Several studies have demonstrated that Lys ligation in the presence of the native Met80 in cyt *c* is also possible at near neutral pH (Table S1).[23–29] Destabilization of the heme coordination loop is the likely explanation for the decreased pK_a of the alkaline transition for several mutants of cyt *c* that target this loop, as well as for the presence of Lys-ligated conformers for cyt *c* in the presence of urea.[4] Mechanistic studies have suggested that deprotonation of a yet unknown "trigger" group precedes ligand replacement.[14,15] Analysis of the recent structure of the Lys-ligated T78C/K79G cyt *c* variant has revealed that changes at residue 78 modify the hydrogen-bonding interactions in the vicinity of this site.[22] These changes affect the environment of the trigger group and prime the heme coordination loop for refolding. Evidently, minor perturbations in protein structure (in this variant, through changes in sequence) appear to mediate the switch between the Lys-ligated and Met-ligated conformations.

Herein, we focus on two residues, Thr49 and Tyr67, to further evaluate the significance of certain tertiary contacts for maintenance of the native structure and ligation. These residues do not belong to the heme coordination loop but are highly conserved among mitochondrial cyt *c* proteins[3] and, similar to Thr78, contribute to the extensive hydrogen-bonding network that defines the skeleton of the protein (Figure 1).[6] This network mediates cross-talk between regions of different stability (foldons)[19] and has been implicated in regulating both ET and peroxidase activities of cyt *c*.[30–32] Located within the Ω-loop C, Thr49 forms a hydrogen bond with the carboxyl group of heme propionate 6 (HP6). The other residue, Tyr67, is engaged in hydrogen-bonding contacts with both Ω-loops C and D and interacts directly with the heme iron ligand Met80.

Mutations T49V and Y67R in horse heart cyt *c* were chosen to introduce changes in the protein tertiary contacts by disrupting hydrogen bonding and packing of the heme coordination loop, respectively. The T49V mutation was designed to eliminate the Thr49-HP6 hydrogen bond but minimize steric and electrostatic perturbations at this site. In contrast, by selecting a bulky charged Arg residue at position 67,[33] we aimed to perturb as much as possible not only the intraprotein hydrogen-bonding network but also the packing of the nearby heme coordination loop. The previously observed increase in the peroxidase activity of yeast and human Y67R cyt *c* was a hint to the major structural perturbation associated with this mutation.[30,34]

Spectroscopic studies described in this report reveal that both variants are Lys-ligated at neutral pH. Thermodynamic stability measurements, kinetics of Lys binding and dissociation, and the pH-dependent changes in ligation provide detailed characterization of the Lys coordination in these distinct variants and relate these properties to the extent of structural perturbations. Our findings emphasize the importance of the hydrogen-bonding network in cyt *c* in controlling the native Met80 ligation to the heme iron.

Materials and Methods

Chemicals were purchased from Fisher Scientific Inc., unless noted otherwise. Buffers were prepared using reagent-grade chemicals. Water was purified to a resistivity of 18 MΩ cm using Barnstead E-Pure Ultrapure Water Purification System. Data analyses were carried out using MATLAB 2011a-2015a (MathWorks), SigmaPlot 10.0 (Systat Software), and Origin 8 (OriginLab Corporation).

Site-Directed Mutagenesis, Protein Expression and Purification

Point mutations in the pBTR plasmid[35] encoding horse heart cyt *c* were introduced using a Quikchange kit (Agilent). Mutations were confirmed by sequencing at the Molecular Biology & Proteomics Core Facility (Dartmouth College). Expression and purification of the proteins were performed as described previously.[8] Wild-type horse heart cyt *c* (WT) was purchased from Sigma-Aldrich (C2506) and, similarly to our mutants, purified using ion-exchange chromatography.

Sample Preparations

Ferric and ferrous proteins were prepared by adding excess of potassium ferricyanide and sodium dithionite, respectfully. The excess of the redox reagent was removed using size-exclusion (PD-10 desalting column, GE Healthcare) or ion-exchange (Sepharose HP SP, GE Healthcare) chromatography. Sample preparations of ferrous proteins were performed under anaerobic conditions in a nitrogen-filled glove box (COY Laboratory Products). All ferrous samples were sealed in a cuvette (Starna Scientific) or NMR tube (Wilmad Lab Glass) before taking out of the glove box for spectroscopic measurements.

Spectroscopic Measurements

All the experiments were performed at room temperature of 22 ± 2 °C unless specified otherwise. Electronic absorption spectra were acquired on an Agilent 8453 diode-array and JASCO V-630 scanning spectrophotometers. Circular dichroism (CD) spectra and CD temperature melting curves were recorded on a JASCO-J815 CD spectropolarimeter equipped with a variable temperature peltier cell device (JASCO, Inc.). Pyridine hemochrome assays were conducted to determine the extinction coefficients of the prepared variants.[36]

Low temperature (10 K) EPR spectra were recorded on a Bruker EMX 300 X-band EPR spectrometer (Bruker Biosciences Corp.). Experimental parameters were set to 9.49 GHz microwave frequency, 3.21 mW microwave power, 100 kHz modulation frequency, 1.00 G modulation amplitude and a 20.48 ms time constant. Protein concentrations were between 200–500 μM and samples contained 30% v/v of glycerol, unless otherwise noted. All EPR data were analyzed using Bruker WinEPR V2.22 Rev.10.

^{1}H NMR spectra were recorded on a 500 MHz Bruker NMR spectrometer (Bruker Biosciences) at 25 °C. The ferric proteins were prepared in 100% D_2O, while the ferrous samples contained 10% (v/v) D_2O; 50 mM sodium phosphate or sodium d_6-acetate were used to buffer these solutions. Protein concentrations were around 500 μM and the buffers

were exchanged by repeated ultrafiltration using 10 kDa centrifugal ultrafiltration devices (Millipore). Sodium dithionite (1 mM) was kept in the solution for NMR measurements of samples of ferrous proteins. With ferrous proteins, excitation sculpting with gradients was used to suppress water in 1D ^{1}H NMR or 2D ^{1}H NOESY experiments. With ferric proteins, 1D ^{1}H NMR spectra were collected using a superWEFT pulse sequence[37] with a recycle delay of 220 ms for low-spin heme species of cyt *c* or 110 ms for high-spin heme species. All NMR data were analyzed using Bruker TopSpin 3.2.

Spectroelectrochemical Measurements

Spectroelectrochemistry experiments were performed as previously described.[38] The absorbance of cyt *c* samples at 550 nm was plotted as a function of external potentials and fitted to eq 1, where A_m is the absorbance of the 100% ferrous protein; E° is the heme iron reduction potential; and n is the number of electrons transferred in the reaction.

$$f(x)=\frac{A_m}{10^{\left(\frac{x-E^\circ}{1000}\times\frac{n}{0.059}\right)}+1} \quad (1)$$

Thermal Denaturation

CD ellipticity at 222 nm were recorded in the temperature range of 20–90 °C. Proteins were prepared at concentrations between 15–25 μM. Under these conditions thermal denaturation of all the studied cyt *c* variants was ≥83% reversible. Dependencies of CD signal on temperature were fitted to eq 2, where m_f and b_f are the slope and *y*-intercept of the signal from the folded protein; m_u and b_u are the slope and *y*-intercept of the signal from the unfolded protein; R is the gas constant; T_m is the midpoint of the unfolding transition; ΔH is the van't Hoff enthalpy of denaturation at T_m.

$$f(x)=\frac{(m_fT+b_f)+(m_uT+b_u)\exp[(\frac{-\Delta H}{R})(\frac{1}{T}-\frac{1}{T_m})]}{1+\exp[(\frac{-\Delta H}{R})(\frac{1}{T}-\frac{1}{T_m})]} \quad (2)$$

GuHCl Denaturation

A series of GuHCl solutions were prepared by dissolving GuHCl into the appropriate buffer and adjusting the pH to the desired values. The GuHCl concentration of each sample was calculated from the refractive index (ΔN) of the GuHCl sample measured by a digital refractometer.[39]

Changes in the α-helical content were monitored by CD ellipticity at 222 nm as a function of GuHCl concentration. Plots of ellipticity versus GuHCl concentration were fitted to eq 3:[40]

$$f(x)=\frac{(m_f[GuHCl]+b_f)+(m_u[GuHCl]+b_u)\exp(\frac{m_D[GuHCl]-[GuHCl]_{1/2}}{RT})}{1+\exp(\frac{m_D[GuHCl]-[GuHCl]_{1/2}}{RT})} \quad (3)$$

where m_f and b_f are the slope and *y*-intercept of the signal from the folded protein; m_u and b_u are the slope and *y*-intercept of the signal from the unfolded protein; R is the gas constant; T is the experimental temperature; $[GuHCl]_{1/2}$ is the midpoint of the unfolding transition; m_D is the slope of the unfolding transition.

The Gibbs free energy of unfolding was calculated using eq 4:

$$\Delta G_D = m_D \times [GuHCl]_{1/2} \quad (4)$$

pH Titrations and Singular Value Decomposition Analysis

Protein concentrations were around 10–15 μM and 75–100 μM for absorption measurements in the Soret region and the charge-transfer band, respectively. The pH was adjusted using either 1 M sodium hydroxide or 1 M hydrogen chloride, and monitored using an AB15 pH meter (Fisher Scientific).

Singular Value Decomposition (SVD) analyses on pH titration profiles were conducted following previously reported procedures.[41,42] To allow for accurate analysis of the Soret and charge transfer bands, two separate spectral series were constructed: in the 350 nm–650 nm at low protein concentrations and in the 590 nm–720 nm at high protein concentrations. Deconvolution of the pH titration profile A (λ_m, pH_n) into the wavelength dependence vectors $U(\lambda)$, square roots of the eigenvalues S(k) and the pH dependence V(pH) was calculated by using the MATLAB_R2014b SVD function ($A=USV^T$). Log of $S_{j,j}$ values, $S_{j,j}$ percentages $(\frac{S_{j,j}^2}{\sum_{j=1}^{k} S_{j,j}^2}) \times 100\%$, error levels $(\sqrt{\frac{\sum_{j=1}^{k} S_{j,j}^2}{\sum_{j=1}^{k} S_{j,j}^2}})$, autocorrelation of U(λ) and V(pH) matrices were used as criteria to determine the number of significant components, i[41,42]. The selected V-vectors $V_i(pH)$ were then globally fitted to eq 5 using SigmaPlot 10.0, where A_i and B_i are the slope and y-intercept of the ith transition; $pK_{app,i}$ is the apparent pK_a value for the ith transition; C is the constant corresponding to the absorbance of the initial state:

$$f(x)=\sum_i \frac{B_i+A_i \times 10^{pK_{app,i}-pH}}{1+10^{pK_{app,i}-pH}}+C \quad (5)$$

The fractional population changes of the major components, F(pH) were calculated based on the model describing the transition (in this study, two- or three-state, depending on the variant), which were then used to get the spectra of i components D(λ) using eq 6.

$$D = AF^{-1} \quad (6)$$

When a spectrum of a certain component (D_{input}) was used as a constraint, spectra for the rest of the components D_{output} were calculated as $D_{output} = (A - D_{input}F_{input})F_{rest}^{-1}$, where F_{input} is the change in fractional population of the species having the input spectrum and F_{rest} are the changes in fractional populations for the rest of the species. For Y67R/M80A, input-independent analysis was employed. For T49V, the spectrum of the Met-ligated species (WT at pH 7.4) was used as an input D_{input}.

pH-jump and Imidazole Binding Kinetics

Fast kinetics were examined by performing rapid-mixing experiments on a BioLogic SFM-300 stopped-flow instrument using ferric proteins. For pH-jump measurements, the protein samples were prepared in a 5 mM (Y67R/M80A) or 10 mM (T49V) sodium phosphate buffer at pH 7.4 containing 100 mM sodium chloride for downward pH jump or in a 5 mM (Y67R/M80A) or 10 mM (T49V) sodium acetate buffer at pH 4.5 containing 100 mM sodium chloride for upward pH jump experiments. The jump buffers were all 10 mM for T49V and 18 mM for Y67R/M80A (sodium acetate, pH 4.5–5.5; bis-tris, pH 6.0–6.5; MES, pH 6.0–6.2; sodium phosphate, pH 6.5–8.0; boric acid, pH 9.5; CAPS, pH 10.5) with 100 mM sodium chloride. The electronic absorption spectra between 250–600 nm were recorded immediately after mixing of the jump buffers with protein solution by a 5 to 1 ratio. The absorbance changes as a function of time were fitted to monoexponential decay (or rise) functions. The final pH was measured by a UB-10 pH meter (Denver Instrument) with the mixtures of the jump buffers and the protein buffers.

The following mechanistic scheme, adapted from previous studies of cyt *c* alkaline transition,[14] was employed to analyze the pH jump experiments (Scheme 1). The mechanism involves initial deprotonation step of the “trigger” group T of the species with the heme iron ligated by ligand X (H_2O for Y67R/M80A and Met for T49V), followed by a conformational transition to the Lys-ligated species. The rate constant k_f and the protonation equilibrium constant K_H were determined from the fits of the observed k_{obs} to eq 7; the average of the first four points form the pH jump data (low pH) was used to set the rate constant k_b. Eq 7 is derived assuming that the deprotonation equilibrium is fast compared to the conformational transitions.

$$k_{obs} = k_b + k_f \times \frac{K_H}{K_H + [H^+]} \quad (7)$$

The binding of imidazole (Scheme 2) to the T49V and Y67R/M80A variants was studied by examining changes in the Soret absorption band.[43] Protein and imidazole solutions were prepared in a 100 mM sodium phosphate buffer at pH 7.4. Aliquots of the protein solution were added to the solutions of imidazole and the samples were allowed to equilibrate for at least 30 min before recording absorption spectra. The apparent dissociation constant K_D^{app}

and pH-independent dissociation constant K_D value were determined from the fits of these spectral series (eqs 8 and 9).

$$\Delta A = \frac{A_{max}[Im]}{K_D^{app} + [Im]} \quad (8)$$

The pH independent dissociation constant of imidazole binding to the heme iron was calculated according to eq 9, where the acid dissociation constant of the imidazolium K_a is 10^{-7}.

$$K_D = K_D^{app}\left(1 + \frac{[H^+]}{K_a}\right) \quad (9)$$

For the kinetic binding experiments, mixing experiments were conducted using a stopped-flow instrument. Protein samples (50 μM) were prepared in a 100 mM sodium phosphate buffer at pH 7.4 and mixed with a 150 mM imidazole stock solution. The spectra in the range between 250–600 nm were recorded for 60 s after mixing. Changes in absorbance at 413 nm were fitted to monoexponential progress curve functions to yield k_{obs}^{Im}. The rate constants k_{off}^{Lys} and k_{off}^{Im} were then calculated using eq 10.[44]

$$\frac{1}{k_{obs}^{Im}} = \frac{1}{k_{off}^{Lys}} + \frac{K_D}{k_{off}^{Im} + [Im]} \quad (10)$$

Results

Characterization of the Initial Set of Variants

For both ferric T49V and Y67R at pH 7.4, the Soret band maximum is at 406 nm, blue-shifted from its position at 409 nm in WT (Figure 2A). Under these conditions, both mutants lack the 695 nm charge transfer band that is associated with Met80 ligation to the ferric heme iron. The downfield region of the cyt *c* ^{1}H NMR spectrum displays the resonances of the heme methyl groups that are sensitive markers of the heme iron ligation (Figure 2B).[14,20] The two resonances of the 8-CH3 and 3-CH3 protons at around 35 ppm, which correspond to the Met-ligated heme iron in WT under native conditions, are not detectable for Y67R and their intensities are greatly diminished for T49V (Figure 2C). Instead, there are new resonances in the 25–5 ppm region, consistent with the upfield shift of the 8-CH3 and 3-CH3 protons. Previous detailed NMR studies of cyt *c* alkaline conformers have assigned these spectral changes to substitution of the heme iron ligand from the native Met80 to Lys73 or Lys79 at high pH.[14,45] The upfield region of the ^{1}H NMR spectra, where the γ-CH_2 and ε-CH_3 resonances of the Met80 ligand can be found, is also in accord with replacement of the Met80 ligand in the variants at pH 7.4. Under these conditions no Met80-

ligated conformers are present in Y67R but a small population of Met80-ligated species still persists in T49V. The NMR results, together with electronic absorption spectra, suggest that another ligand (most likely Lys) replaces Met80 at the heme iron in these mutants.

The ferrous WT, T49V, and Y67R variants all have very similar electronic absorption spectra typical of low-spin ferrous heme with a neutral ligand (Figure 2A). While the absorption spectra are alike for Met-, Lys-, and His-ligated ferrous heme proteins, the NMR spectra do allow identification of the axial ligand.[46,47] Similar positions of resonances in the 1D ^{1}H spectra (Figure 2D) and pattern of cross-peaks in the 2D NOESY spectra (Figure S1) of ferrous T49V to those of WT, suggest that Met80 is also the ligand of the ferrous heme in this variant at pH 7.4.

The two additional “satellite” resonances, labeled with asterisks in Figure 2D, however, suggest that there is a small population of another species in T49V. A similar set of resonances, yet at lower magnetic field and without accompanying resonances of the Met80-ligated species, is evident in the spectrum of ferrous Y67R. We have hypothesized that the introduced mutations might have led to an opening of the heme pocket and subsequent oxidation of Met80 during the preparation of the two variants. Recent studies of CL-bound human cyt *c* have revealed that molecular oxygen can oxidize Met80 to methionine sulfoxide Met-SO when the heme pocket is perturbed.[48] To test this hypothesis, we have intentionally oxidized Met80 in T49V by treatment with chloramine-T,[49] generating the reference protein T49V-ox. The resonances of Met80-SO of T49V-ox match exactly the resonances of the minor species in the upfield spectra of T49V samples (Figure 2D).

Comparison of the ^{1}H NMR spectra of ferrous T49V and T49V-ox at equal concentrations of proteins suggests that no more than 10% of the protein in our T49V samples have Met80-SO. The electronic absorption (Figure 2A) and NMR (Figure 2C) spectra of ferric T49V-ox are consistent with Lys-ligation to the heme in this modified protein. Since Met80 is replaced at the ferric heme iron by a Lys residue in both T49V and T49V-ox, their conformational properties should be largely the same. Furthermore, because the population of T49V-ox in T49V samples is small, its presence only minimally affects the biophysical properties of T49V in the characterization experiments below.

For Y67R, however, the entire protein population has Met80 oxidized. NMR spectra (Figure 2D), as well as the increased mass of the variant (16.2 ± 4.3 Da) in MALDI spectra, support this conclusion. Since Met oxidation results in a change in the heme iron ligation even for WT, the effects of this modification and the effects of tertiary contact perturbations from the Y67R mutation are difficult to separate. To ensure that the observed changes in structure and properties were due to the point mutation and not Met-SO, a mutation of Met80 was added in the subsequent work to yield the double mutant Y67R/M80A. We have also prepared and characterized M80A as a reference protein in our studies of Lys-ligated variants (Figure S2).

Characterization of Ligation, Structural Properties, and Stability of the Variants at pH 7.4

The electronic absorption spectra of ferric Y67R and Y67R/M80A at pH 7.4 are similar (Figures 2A and 3A). The Y67R/M80A variant does not have a split Q-band, which is apparent for the hydroxide-ligated M80A,[50–52] suggesting that the heme ligand in this

variant is likely not a hydroxide. This conclusion is further supported by NMR spectra (Figure 4A). Spectral signatures of the hydroxide-ligated heme iron species at 16, 14.5 and 13.5 ppm, evident in the spectrum of M80A, are absent in the ^{1}H NMR spectra of Y67R/M80A and T49V. Instead, both Y67R/M80A and T49V display the heme methyl resonances at positions seen with Lys-ligated alkaline cyt *c*.[4] The EPR spectra of Y67R/M80A and T49V are also distinct from the Met-bound WT and the hydroxide-ligated M80A (Figures 4C and S2C)[53] and resemble those of the alkaline WT[14] and the Lys-ligated mutants of cyt *c* and cyt *c*-550.[46] Consistent with the lack of Met80 ligation to the heme, the visible CD spectra of T49V and the two M80A mutants do not have a negative band at 416 nm (Figure S3).[54]

Electronic absorption spectra have revealed that, in contrast to M80A, the ferrous heme in Y67R/M80A is low-spin, indicating that some residue coordinates to the heme in this perturbed variant (Figure 3B). Analysis of the upfield region of the ^{1}H NMR spectrum (Figure S4) suggests that this ligand is Lys.

Reduction potentials obtained from spectroelectrochemistry measurements are in accord with a Lys-bound heme in the T49V and Y67R/M80A variants (Table 1). Upon Lys-coordination, the reduction potential decreases dramatically from the positive value found in wild type (WT, 255 mV),[55] as seen in alkaline WT (−205 mV)[56] and a recently described Lys-ligated variant of cyt *c* (−94 ± 2 mV).[22] The potential of Y67R/M80A is lower than that of T49V. Differences in ligation to the ferrous heme (Lys in Y67R/M80A and Met in T49V) could account for this variation, but other factors, such as changes in the heme exposure, could contribute as well. For Y67R/M80A, the two titration curves from reductive and oxidative experiments do not fully overlap with each other, probably due to some irreversibility in the process.

CD spectra of the variants were compared to evaluate the effects of the mutations on the secondary and tertiary structures of the ferric protein (Figure 5). Consistent with previous findings of minimal structural perturbation with the M80A mutation, the spectra of WT and M80A are very similar. The spectra of the two other mutants, however, suggest changes in the protein conformation. In the far-UV region, the dominant α-helical features of cyt *c* are still apparent but the changes in the shapes of the spectra suggest an increase in the random-coil character. In the near-UV region, the CD signals of the two mutants are greatly diminished compared to the two reference proteins, suggesting variations in their tertiary structure, which are particularly prominent in Y67R/M80A.

Thermal and chemical denaturation of the ferric variants was examined with CD spectroscopy (Table 2). Thermodynamic parameters for WT[57] and M80A are remarkably similar, suggesting that Met coordination has little to no contribution to the global stability of the protein. For T49V, the T_m and ΔH values from thermal denaturation and the $[GuHCl]_{1/2}$ and ΔG_f values from GuHCl denaturation experiments are also similar to that of WT. These results suggest that the favorable binding interactions between Lys and the heme iron may compensate for the destabilizing effect of removing the hydrogen bond between Thr49 and HP6. The T_m, ΔH, and ΔG_f values for Y67R/M80A are the lowest in the set of variants studied.

Characterization of Ligation, Structural Properties, and Stability of the Created Variants at pH 4.5

A decrease in solution pH introduces notable changes in the spectra and stability of the ferric variants. At pH 4.5, the electronic absorption, NMR, and EPR spectra of WT are unchanged (Figure 6). The Soret band in the electronic absorption spectra of M80A and Y67R/M80A blue shifts to 400 nm and the charge transfer bands characteristic of the high-spin H_2O-coordinated heme iron appear. The ^1H NMR spectra of these M80A variants are also consistent with a change in the heme iron spin state with lower pH, as the high-spin heme iron species is readily apparent in the downfield region of the spectra (Figure S5). The EPR spectra show two sets of *g*-values corresponding to the high-spin and low-spin heme iron species (Figure 6C). At this pH, both sets of signals likely arise from the H_2O-ligated heme iron species.[58] A similar pair of EPR signals has been reported previously for H_2O-ligated AcMP8 at pH values where the H_2O ligand should remain protonated.[59] The explanation based on the positioning of the *d*-orbital levels for the mixture of the two states in H_2O/His-ligated hemes has been previously proposed.[59,60]

The Soret band of T49V at pH 4.5 shows a drop in intensity as well as a small red shift of λ_{max} (from 406 to 407 nm) compared to those at pH 7.4 (Figures 6A and 3A). The charge transfer band at 695 nm that was lacking at pH 7.4 reappears but its intensity is less, relative to that of WT. In addition, the charge transfer band at 624 nm is also present. In contrast to the NMR spectrum at pH 7.4 (Figure 4A), the NMR spectrum of T49V at pH 4.5 does not display the diagnostic resonances of Lys ligation at 10–25 ppm (Figure 6B). Instead, the heme methyl resonances at around 35 ppm appear at positions similar to those in the WT spectrum. A small signal in the downfield region of the NMR spectrum, indicative of the high-spin heme iron species, is also apparent (Figure S5). EPR spectra of WT and T49V are also similar (Figure 6C); a smaller population of the high-spin species in the EPR spectra at 10 K, compared to that in the electronic absorption spectra at room temperature, is likely related to temperature effects. Collectively, all three spectroscopic methods point to the presence of the major population of the Met-ligated species and a minor population of the H_2O-ligates species in the T49V ensemble at this low pH. The thermodynamic stability parameters from thermal denaturation experiments suggest that the mutant becomes less stable at pH 4.5 (Table 2). However, given the presence of at least two types of species (with Met- and H_2O-ligated heme iron), the classic two-state model may oversimplify the T49V unfolding transition under these conditions.

The increase in reduction potentials at pH 4.5 is consistent with the spectroscopic findings of a Met-ligated species for T49V and a high-spin H_2O-ligated species for Y67R/M80A (Table 1). These ligation changes are largely responsible for the increase in reduction potentials, with additional contributions arising from the change in electrostatic interactions at lower pH, described previously for cyt *c*,[3,61] adding to these effects.

pH-Dependent Changes in Ligation

Our experiments have revealed that Lys ligates to the heme iron in both T49V and Y67R/M80A at pH 7.4 but it is no longer the heme ligand at pH 4.5. In order to understand the mechanisms of these pH-dependent changes in ligation, we next examined changes in the

electronic absorption spectra of these variants over a wider pH range and performed SVD analyses to figure out the number of major species in the spectral series, identify their spectra, and also determine the pK_a values of conformational transitions.

Multiple criteria of matrix analysis (see Materials and Methods) consistently indicated that the series of spectra for T49V can be described by three components, while Y67R/M80A required only two components. Global fitting of the selected V_i(pH) vectors (V-vectors) to eq 5 yielded pK_a values in Table 3. The same results were obtained from analyses of the pH profiles separately recorded in the 350–500 nm (Soret band; Figures 8 and 9) and 590–720 nm (charge transfer (CT), Figures S6 and S7) spectral regions.

For T49V, the pK_a value of the low pH transition is in a good agreement with the value previously found for the transition of the native Met-ligated conformation to the H_2O-ligated acidic conformation of WT cyt *c*.[62] These two species are likely two of the three components from SVD analysis of T49V spectra. This conclusion is consistent with the signatures of Met- and H_2O-ligated species apparent in the spectra of T49V at low pH (Figure 6). The abundant evidence for the Lys-ligated conformer from our spectroscopic and electrochemical characterization of T49V at pH 7.4 suggests that this species should be the third component. Since the Met80 residue was replaced by a non-coordinating Ala in Y67R/M80A, there is no Met-ligated species and the two components revealed from the analysis of this mutant are conformers with H_2O- and Lys-ligated heme iron.

Because the electronic absorption spectra of the Lys- and hydroxide-ligated cyt *c* are similar (Figure 3A), we first considered the possibility that the SVD analysis of these data might have missed this additional heme species. The NMR and EPR measurements ruled out the presence of the hydroxide-ligated heme iron for both T49V and Y67R/M80A at pH 7.4. Experiments at pH 10.5 suggest that, similar to alkaline WT, it is Lys, rather than hydroxide, that coordinates the heme iron under these conditions as well (Figure S8). To evaluate whether the hydroxide-ligated species plays a role in the pH range between 4.5 and 7.4 when the Lys ligation is being lost, we have examined the pH dependence of the ^{1}H NMR and EPR spectra of the two mutants.

For T49V, the heme methyl resonances between 15 ppm and 25 ppm, which are characteristic of protein conformers with Lys-ligated heme iron, are absent in the ^{1}H NMR spectra below pH 5.0, and are barely detectable at pH 6.0 and pH 6.5 (Figure S9). The resonances around 35 ppm, which are diagnostic of Met-ligated conformers, are apparent in the pH range from 4.5 to 6.5. As the pH increases from 7.4 to 8.2, these signals decrease in intensity and completely disappear at pH 9.2. The Lys-ligated species is the dominant species at neutral and alkaline pH. ^{1}H NMR spectra between 15 ppm and 25 ppm reveal no evidence of the ferric heme ligated by the hydroxide ligand. The signal associated with the hydroxide-ligated form (g_z=2.58) is absent from the EPR spectrum over the entire pH range as well. The intensities of the NMR and EPR signals associated with Met- and Lys-ligation fit nicely along the pH titration curve from the SVD analysis of the electronic absorption data (Figure 7). These findings further strengthen our assignment of the conformational transition with a pK_a of 6.8 to switch between Met and Lys-ligated conformers, and illustrate the robust nature of our analysis.

A similar conclusion of the lack of hydroxide-ligated heme species in the pH range of the transition can be drawn from the analysis of ^{1}H NMR and EPR spectra of Y67R/M80A (Figures 7 and S10). The heme methyl resonances characteristic of the hydroxide-ligated species are readily apparent in the pH-dependent NMR spectra of M80A (Figure S2) but there are no such signals in the Y67R/M80A spectra (Figure S10B). At pD 5.7, near the pK_a value from the electronic absorption data, the resonances between 15 ppm and 25 ppm associated with Lys-ligated conformers are apparent in the Y67R/M80A spectra, consistent with a Lys and not a hydroxide, ligand participating in the transition to the species with the water-ligated heme iron. The pK_a values of the coordinated water in proteins with His/H_2O-ligated heme iron vary widely;[51] the pK_a=6.1 for M80A (Table 3 and Figure S2) is among the lowest values reported. The protein environment is responsible for dramatic lowering the pK_a of the water ligand in this protein; when these constraints are removed in microperoxidase-8, the pK_a increases to 9.6.[59] We argue that if hydroxide is the heme ligand in the structurally perturbed Y67R/M80A, then the pK_a of the water to hydroxide should have been >6.1 and we would have seen this species, rather than Lys-ligated species, at the titration midpoint. Based on the spectra and these pK_a arguments, we conclude that Lys is replaced by H_2O and there is no sizable population of the hydroxide-ligated heme iron in the pH range of the transition.

Our SVD analysis combined with the above control experiments, indicate that pH-dependent transitions involve H_2O-, Met-, and Lys-ligated species for T49V and H_2O- and Lys-ligated species for Y67R/M80A. The case of Y67R/M80A is more trivial (Figure 10a): calculations of conformer populations using the two-state model yield the component spectra in Figure 9D. The spectrum of the low-pH component strongly resembles that of water-ligated M80A at pH 4.5 and is even closer to the spectrum of M80A under molten-globular conditions. These results are in accord with our ligand assignment and findings of the flexible tertiary structure from CD studies of the mutant (Figure 5B).

The case of T49V, for which there are three components, suggests a sequence depicted in Figure 10B. The two pK_as correspond to transitions from Lys- to Met- and then from Met- to water-ligated heme iron species. The following experimental findings argue in favor of this model. The titrations monitoring the charge-transfer spectral region have revealed that at pH=5, more than one pH unit away from either of the two pK_a values, the spectral properties of T49V and WT are very similar (Figure S6C), suggesting that the population of the Met-ligated species in T49V is close to 100% under these conditions. Furthermore, the NMR and EPR titrations also suggest a clean conversion of the Lys- to the Met-ligated species, without the presence of the water-ligated species along the way.

The spectra of the H_2O- and Lys-ligated components (Components 1 and 3, respectively) derived from the SVD analysis of T49V pH titrations show high similarities, both in the positions and the relative intensities of the Soret bands, to that of the reference spectra (Figure S11). However, the Soret band in the calculated spectrum of the Met-ligated species (Component 2) is blue shifted compared to that of WT. A possible explanation for this discrepancy is that the similar spectral features of the Met- and Lys-ligated forms may not be well resolved to yield distinct spectra in the pH titration profile analysis.

To address this issue, the WT spectrum was used as an input for Component 2, restricting the matrix calculations of the spectra of the two other components (Figure 8D). The resulting spectrum of the Lys-ligated heme species (Component 3) matches well that of WT at alkaline pH. The calculated spectrum of the H_2O-ligated species (Component 1) is also similar to that of the H_2O-ligated M80A reference. In contrast to Y67R/M80A, the spectrum of the folded M80A at pH 4.5 is a better match for the water-ligated T49V than that of the molten-globular M80A form, consistent with the differences in the tertiary structure of the two variants.

pH-Jump Kinetics and Lys Dissociation Rates from Imidazole Binding Experiments

Time-dependent changes in the absorption spectra of the Y67R/M80A and T49V variants upon downward and upward pH jumps yielded kinetic parameters for the transition to the Lys-ligated conformations (Table 4). All kinetics progress curves from these experiments could be described by single-exponential functions (Figure S12). The k_{obs} values show a clear dependence on pH conditions (Figure 11). According to eq 7, at low pH, where $[H^+] >> K_H$, the k_{obs} is dominated by the k_b value. At very high pH, where $K_H >> [H^+]$, $k_{obs} = k_f + k_b$.

The conformational equilibrium constants, K_C, obtained from the ratios of the forward k_f and reverse k_b rate constants allowed the apparent pK_a values to be calculated (Table 4); these values agreed well with the pK_a values from pH titrations (Table 3). For Y67R/M80A and T49V, changes in both the conformational equilibrium constant K_C and the acid dissociation constant of the transition "trigger" group, K_H contribute to lowering the apparent pK_a. Evidently, the mutations in these two variants not only affect the equilibrium associated with Lys ligation but also perturb the protein conformation in close vicinity of the trigger group.

The rate constants k_f for the formation of the Lys-ligated species of the two mutants are very similar to that of WT. In contrast, clear differences are seen in the rate constants k_b for the back conversion from the Lys-ligated species. The differences in k_b correlate with the differences in the protein tertiary structure for WT and the two mutants (Figure 5B). The Lys-ligation is lost most readily in Y67R/M80A, the protein variant with a flexible tertiary structure and greatly diminished thermodynamic stability.

Both Y67R/M80A and T49V bind imidazole as evidenced by concentration-dependent changes in the absorption spectra. At high imidazole concentrations $[Im] >> K_D$, the rate constants k_{obs}^{Im} are independent of the concentration of the exogenous ligand. The expression for k_{obs}^{Im} in eq 10 explains the observed independence of k_{obs}^{Im} $(\text{and } 1/k_{obs}^{Im})$ on imidazole concentration at high concentrations of imidazole as the term $\frac{K_D}{k_{off}^{Im}+[Im]}$ becomes negligible. The calculations of this term using the previously determined $k_{off}^{Im} = 2.4\ s^{-1}$ for cyt c^{44} are in accord with this conclusion. The rate constants k_{obs}^{Im} from imidazole binding experiments are within error bounds of the pH jump k_b values (Table 4), suggesting that the rate constant k_b reports on the Lys dissociation from the heme iron.

Discussion

Mutants in This Work

Mutational studies of cyt *c* have provided critical information about the folding and redox properties of this widely-studied protein. Residue 49 is either Thr or Ser in mitochondrial proteins.[3] While structural data exist only for Thr49 proteins, presumably both amino acids could engage in hydrogen bonding with HP6. Before our work, there has been only one report of a Thr49 mutant.[63] The yeast *iso*-1 cyt *c* T49K mutant has been shown to support oxidative phosphorylation in yeast cells deficient in their ability to produce other isoforms of cyt *c*, but no biophysical characterization of this variant has been performed.

Residue 67 is Tyr in all species, with the exception of *Euglena gracilis*, in which Phe takes its place.[3] Tyr67 was the subject of several mutational studies, and replacements at this site affected the protein stability, the heme iron reduction potentials, and ET kinetics.[31,32,64–68] Notably, the mutation Y67R increases the protein peroxidase activity in both yeast and human proteins,[30,34] suggesting a possible involvement of residue 67 in a functional switch of cyt *c* from electron carrier to a peroxidase. The loss of the native Met80 ligation to the heme iron and the decrease in the protein's thermal stability have been linked to the higher intrinsic peroxidase activity of this variant compared to that of WT.

Alkaline Transition and Trigger Groups

Our studies have revealed that both T49V and Y67R/M80A mutations lower the pK_a of the alkaline transition in cyt *c*, resulting in a population of the Lys-ligated species already at neutral pH. In accord with our findings,[34] recent resonance Raman experiments have identified a population of the Lys-ligated species in human Y67R cyt *c* at pH 7.0. Hydrogen exchange experiments have demonstrated that the pK_a value of the alkaline transition correlates with the stability of the heme coordination loop,[23] and this parameter has been frequently employed to evaluate the properties of the heme crevice.[16] Over the years, an extensive library of cyt *c* mutants has been made for which pK_a values for this transition were determined (Table S1).[3,14,23–29,58,65,69–80] Owing to specific interests of the investigators, most of the mutations have targeted the heme coordination loop but several other specific contacts have been probed. Despite limited sampling of possible perturbations in the set, its inspection provides some insights (Figure 12 and Table S1). Not surprisingly, mutations at the heme coordination loop strongly affect the transition pK_a, where introduction or removal of a bulky residue has the largest impact. However, mutations in the Ω-loop C and at or near Tyr67 also perturb the transition pK_a. Interestingly, mutations in these regions either decrease or increase the pK_a value of the alkaline transition, suggesting the subtle balance among the different interactions that control stability of these sites and their communications with the heme coordination loop.

The Ω-loop C is the least stable foldon of mitochondrial cyt *c* and is the first to unfold.[81] The hydrogen-bonding network connects this foldon to the heme group and the surrounding coordination loop, and includes a hydrogen-bond between Thr49 and HP6. The internally located Tyr67 is also a part of this extensive network and connects to both Ω-loop C (Asn52) and the heme coordination loop (Thr78 and Met80). Again, there is connectivity to the heme

propionate HP6, which has been suggested as a possible candidate for a trigger group.[16] The pK_a value of HP6 has been proposed to be unusually high (≥9) in WT cyt *c*, compared to the values between 5 and 6 in other proteins.[3,82,83] If this high value is due to structural constraints, disruption of the hydrogen-bonding interactions to HP6 could shift its pK_a closer to the typical values. The decrease in the pK_H values for T49V and Y67R/M80A support this hypothesis. A more dramatic change is expected for the latter mutant, whose structure is majorly perturbed.

While removal of the Thr49-HP6 hydrogen bond does not affect the protein global stability (compare WT and Met-ligated T49V at pH 4.5), it greatly perturbs the local stability of the heme coordination loop. Recent studies of Bowler and coworkers report a similar trend for the two mutants of human cyt *c* Y46F and S47T;[77] however, the effects at these sites are less dramatic than those for T49V. The two mutated residues in Bowler's study also contribute to the intraprotein hydrogen-bonding network, in which the hydroxyl group of Tyr46 is hydrogen-bonded to the carbonyl of Thr28 and the main-chain carbonyl of Ser47 is hydrogen-bonded to the ε-amino group of Lys79. Without kinetic data, it is unclear whether these mutations affect the conformational equilibrium constant (K_c) or also influence the properties of the trigger group (K_H).

The fact that removal of the hydrogen bond in Y67F increases rather than decreases the pK_a value for the transition to the Lys-ligated form[65] suggests that in the case of the Y67R/M80A variant it is a major disruption in the protein structure rather than simply removal of one (or several) hydrogen-bonding interactions that favors the cyt *c* switch to the alkaline form. This situation is reminiscent of that of urea-denatured cyt *c*.[4] The finding of Lys ligation in these highly flexible conformational forms highlights the importance of the protein scaffold for the native Met80 ligation in the ferric protein. Without the proper positioning of Met80, the stronger base Lys within the flexible loop coordinates to the heme iron. When Met80 is no longer available, as in M80A, but the integrity of the rest of the protein structure is preserved, H_2O or hydroxide, rather than Lys coordinate to the heme. Consistent with only minor contribution of the Met-iron bond to the stability of the ferric protein, the thermodynamic stabilities of M80A and WT are very similar.

The apparent pK_a for the alkaline transition is low in Y67R/M80A because of the favorable equilibrium to the Lys-ligated form (pK_c) and because of the low pK_a of the trigger group (pK_H). The deprotonation that controls the transition cannot simply be that of the Lys sidechain since its pK_a (pK_H=6.8 ± 0.4) is much lower than the typical pK_a value of Lys.[84] A trigger group therefore must be involved and this result implies that some structural constraints are still present in the significantly destabilized Y67R/M80A.

For this mutant, the transition involves a switch from H_2O to Lys. The pK_H value is consistent with the pK_a value of the iron-bound water ligand (Table 3). While we have no evidence for the population of the hydroxide-bound heme iron species at equilibrium within the transition range, such species could form transiently. The role of the hydroxide-bound species as an intermediate in the alkaline transition has been previously argued.[75,85] The structure of the cyanide adduct of the horse heart ferric cyt *c* has revealed that the binding of this small negatively-charged ligand is associates with the repositioning of the loop residues

77–85 and expulsion of the native Met80 ligand from the heme crevice.[86] A crystal structure of the hydroxide-bound yeast *iso*-1 K72A cyt *c* reports more modest structural perturbations of the heme coordination loop, but perturbations are still there, primarily affecting Met80, Ala81, and Gly83.[85]

If indeed the deprotonation of the H_2O ligand is what drives the transition to the Lys-ligated species in Y67R/M80A, this has to be linked to increased dynamics of the heme coordination loop, since a similar deprotonation does not cause Lys coordination in M80A. The unfolding of the heme coordination loop is essential for the switch to Lys ligation in alkaline cyt *c*. Perhaps with the flexible tertiary structure of Y67R/M80A its heme coordination loop is mostly unfolded and the change in the heme spin state associated with the H_2O deprotonation is sufficient for Lys to readily coordinate the heme.

In contrast, in WT and variants with less invasive mutations, another deprotonation is required for loop unfolding. Besides HP6, a buried water molecule, Tyr67, and His18 have been proposed as trigger groups for the alkaline transition, and, the second, inner, heme propionate HP7 is another possibility.[16] Analysis of the pH jump kinetics of His-ligated mutants of yeast *iso*-1 cyt *c* suggested that more than one trigger group might be involved. The role of the internal water molecule that hydrogen-bonds to Ty67 and Thr78 (Wat166, Figure 1) in triggering the transition, has been strongly argued in a study of a family of M80X mutants.[58] In ferric yeast *iso*-1 Y67F cyt *c*, this water molecule cannot be located,[68] presumably because of its increased mobility within a larger internal cavity, and the pK_a of the alkaline transition is higher (Table S1).[65] Although this argument provides a possible explanation for the elevated pK_a in the Y67F mutant, the increased stability of the mutant is another factor.[67] It remains to be determined whether HP6, Wat166 or some other group triggers the transition. However, based on our mutational studies, we can already conclude that the integrity of the intraprotein hydrogen-bonding network, particularly the region next to HP6, has prime importance in favoring the native Met-ligated structure of ferric cyt *c* over the Lys-ligated conformers.

Met Oxidation

The development of highly efficient expression systems has led to a recent explosion of mutational studies on cyt *c* from many different species. Designed to probe classical questions in cyt *c* structure-function relationships, some of these mutations dramatically modify the native heme crevice. Studies of CL-bound cyt *c* have shown that molecular oxygen can readily oxidize Met80 to Met-SO, without the requirement of any other enzymes.[48] In this work we have observed stoichiometric oxidation of Met80 in horse heart Y67R cyt *c* during protein expression. It is not clear whether a similar oxidation reaction may have complicated previous studies of yeast *iso*-1 and human cyt *c*.[30,34]

These oxidation reactions appear to depend on the stability of the variants, a property that cannot be easily assessed before the actual experiments. In our earlier work, attempts to recombinantly make yeast M80C variants have yielded proteins with an oxidized Cys80 side chain that did not ligate as a thiolate to the ferric heme iron upon oxidation.[38] In contrast, recombinant expression of the more stable horse heart cyt *c* resulted in thiolate-bound

species. Careful characterization of mutant samples is critically important, since these unintended oxidation reactions can greatly affect the very phenomena one wishes to explore.

Functional Significance

Could the perturbation-induced switch to Lys-ligated conformations at neutral pH be biologically relevant? Previous studies have argued for a link between the protein surface and the redox properties of the heme.[87] Neither residue 49 nor other residues in the Ω-loop C interact with cyt *c*'s physiological redox partners cyt *c* peroxidase,[88] bc_1 complex,[89] and cyt *c* oxidase.[90] The Ω-loop C, however, appears to be relevant for the cyt *c* function in apoptosis as it forms contacts with Apaf-1, as well as with the antiapoptotic protein Bcl-x_L,[91] and belongs to one of the suggested CL- binding site in cyt *c*.[10] The crystal structure of Lys-ligated T78C/K79G suggests that the acyl chain of CL could fit into the hydrophobic pocket next to this helix.[22] Binding to CL membranes perturbs the native protein structure and appear to favor the switch cyt *c* to the Lys-ligated state. Importantly, disruption of the native Met80 ligation modulates peroxidase activity of cyt *c*,[22,85,92] which is important in early stages of apoptosis.

The Ω-loop C is also the region for the mutations G41S and Y48H in human cyt *c*, which are associated with thrombocytopenia.[93,94] The former mutant has been better studied. While there are only subtle changes in the structure of this mutant, there are clear changes in its dynamics that increase ET rates and peroxidase activity.[95,96] Even though G41S cyt *c* is Met-ligated at neutral pH (the pK_a value for the alkaline transition is 7.8±0.3, Table S1),[28] this mutant is primed for ligand replacement. As in the T49V mutant in our study, mutation-induced perturbations in the Ω-loop C affect the heme coordination loop illustrating cross-talk between the two loops. The site and the nature of the perturbation define the extent of the effect on the alkaline transition: with a seemingly minor change in T49V, the pK_a shift is very dramatic and different replacements at residue 41 have varied effects on the transition pK_a (Table S1).

The significance of perturbations at residue 67 is less clear. This internally-located residue plays a structural role and modifications at this site dramatically modify protein dynamics.[31,32] Since the residue is connected through the hydrogen-bonding network to both the Ω-loop C and the heme coordination loop, the possibility for communications with the protein surface exists.

Conclusions

Our spectroscopic studies have revealed that ferric forms of T49V and Y67R/M80A horse heart cyt *c* variants are Lys-ligated already at neutral pH. The change in ligation is linked to structural perturbations. The integrity of the protein scaffold is critical for maintenance of the native Met80 ligation to the heme, allowing cyt *c* to properly function as an electron carrier in oxidative phosphorylation. Interestingly, a minor modification in protein structure owing to disruption of the conserved hydrogen-bonding contact(s) in T49V, away from the ligand and the heme coordination loop, is sufficient to trigger the switch to the Lys-ligated form. These findings illustrate the existence of the cross-talk between the different regions of

the cyt *c*'s structure and strengthen the proposal for the role of heme propionates in the mechanism of alkaline transition in cyt *c*.[16]

Supplementary Material

Refer to Web version on PubMed Central for supplementary material.

Acknowledgments

We thank Kara L. Bren for the horse heart cyt *c* plasmid and Kevin R. Hoke for numerous discussions about cyt *c* electrochemistry.

Funding

The funding for this work was provided by the National Science Foundation (CAREER CHE-0953693 to E.V.P.) and the National Institutes of Health (R01-GM098502 to E.V.P.).

References

1. Miyashita O, Wolynes PG, Onuchic JN. Simple energy landscape model for the kinetics of functional transitions in proteins. J Phys Chem B. 2005; 109:1959–1969. [PubMed: 16851180]
2. Belikova NA, Vladimirov YA, Osipov AN, Kapralov AA, Tyurin VA, Potapovich MV, Basova LV, Peterson J, Kurnikov IV, Kagan VE. Peroxidase activity and structural transitions of cytochrome *c* bound to cardiolipin-containing membranes. Biochemistry. 2006; 45:4998–5009. [PubMed: 16605268]
3. Moore, GR., Pettigrew, GW. Cytochromes c: Evolutionary, structural, and physicochemical aspects. Springer-Verlag; New York: 1990.
4. Russell BS, Melenkivitz R, Bren KL. NMR investigation of ferricytochrome *c* unfolding: Detection of an equilibrium unfolding intermediate and residual structure in the denatured state. Proc Natl Acad Sci USA. 2000; 97:8312–8317. [PubMed: 10880578]
5. Pletneva EV, Gray HB, Winkler JR. Many faces of the unfolded state: Conformational heterogeneity in denatured yeast cytochrome *c*. J Mol Biol. 2005; 345:855–867. [PubMed: 15588831]
6. Bushnell GW, Louie GV, Brayer GD. High-resolution 3-dimensional structure of horse heart cytochrome *c*. J Mol Biol. 1990; 214:585–595. [PubMed: 2166170]
7. Kagan VE, Tyurin VA, Jiang J, Tyurina YY, Ritov VB, Amoscato AA, Osipov AN, Belikova NA, Kapralov AA, Kini V, Vlasova II, Zhao Q, Zou M, Di P, Svistunenko DA, Kurnikov IV, Borisenko GG. Cytochrome *c* acts as a cardiolipin oxygenase required for release of proapoptotic factors. Nat Chem Biol. 2005; 1:223–232. [PubMed: 16408039]
8. Hanske J, Toffey JR, Morenz AM, Bonilla AJ, Schiavoni KH, Pletneva EV. Conformational properties of cardiolipin-bound cytochrome *c*. Proc Natl Acad Sci USA. 2012; 109:125–130. [PubMed: 22190488]
9. Hong Y, Muenzner J, Grimm SK, Pletneva EV. Origin of the conformational heterogeneity of cardiolipin-bound cytochrome *c*. J Am Chem Soc. 2012; 134:18713–18723. [PubMed: 23066867]
10. Muenzner J, Pletneva EV. Structural transformations of cytochrome *c* upon interaction with cardiolipin. Chem Phys Lip. 2014; 179:57–63.
11. Elöve G, Bhuyan AK, Roder H. Kinetic mechanism of cytochrome *c* folding: Involvement of the heme and its ligands. Biochemistry. 1994; 33:6925–6935. [PubMed: 8204626]
12. Bradley JM, Silkstone G, Wilson MT, Cheesman MR, Butt JN. Probing a complex of cytochrome *c* and cardiolipin by magnetic circular dichroism spectroscopy: Implications for the initial events in apoptosis. J Am Chem Soc. 2011; 133:19676–19679. [PubMed: 22081937]
13. Theorell H, Åkesson Å. Studies on cytochrome *c*. III Titration curves. J Am Chem Soc. 1941; 63:1818–1820.

14. Rosell FI, Ferrer JC, Mauk AG. Proton-linked protein conformational switching: Definition of the alkaline conformational transition of yeast *iso*-1-ferricytochrome *c*. J Am Chem Soc. 1998; 120:11234–11245.
15. Martinez RE, Bowler BE. Proton-mediated dynamics of the alkaline conformational transition of yeast iso-1-cytochrome *c*. J Am Chem Soc. 2004; 126:6751–6758. [PubMed: 15161303]
16. Cherney MM, Bowler BE. Protein dynamics and function: Making new strides with an old warhorse, the alkaline conformational transition of cytochrome *c*. Coord Chem Rev. 2011; 255:664–677.
17. Theorell H, Åkesson Å. Studies on cytochrome *c*. II. The optical properties of pure cytochrome *c* and some of its derivatives. J Am Chem Soc. 1941; 63:1812–1818.
18. Döpner S, Hildebrandt P, Rosell FI, Mauk AG, von Walter M, Buse G, Soulimane T. The structural and functional role of lysine residues in the binding domain of cytochrome *c* in the electron transfer to cytochrome *c* oxidase. Eur J Biochem. 1999; 261:379–391. [PubMed: 10215847]
19. Hoang L, Maity H, Krishna MM, Lin Y, Englander SW. Folding units govern the cytochrome *c* alkaline transition. J Mol Biol. 2003; 331:37–43. [PubMed: 12875834]
20. Assfalg M, Bertini I, Dolfi A, Turano P, Mauk AG, Rosell FI, Gray HB. Structural model for an alkaline form of ferricytochrome *c*. J Am Chem Soc. 2003; 125:2913–2922. [PubMed: 12617658]
21. Tezcan FA, Winkler JR, Gray HB. Effects of ligation and folding on reduction potentials of heme proteins. J Am Chem Soc. 1998; 120:13383–13388.
22. Amacher JF, Zhong F, Lisi GP, Zhu MQ, Alden SL, Hoke KR, Madden DR, Pletneva EV. A compact structure of cytochrome *c* trapped in a lysine-ligated state: loop refolding and functional implications of a conformational switch. J Am Chem Soc. 2015; 137:8435–8449. [PubMed: 26038984]
23. Maity H, Rumbley JN, Englander SW. Functional role of a protein foldon – An Omega-Loop foldon controls the alkaline transition in ferricytochrome *c*. Proteins-Struct Funct Bioinformatics. 2006; 63:349–355.
24. Pearce LL, Gartner AL, Smith M, Mauk AG. Mutation-induced perturbation of the cytochrome-*C* alkaline transition. Biochemistry. 1989; 28:3152–3156. [PubMed: 2545249]
25. Black KM, Wallace CJA. Probing the role of the conserved beta-II turn Pro-76/Gly-77 of mitochondrial cytochrome *c*. Biochem Cell Biol. 2007; 85:366–374. [PubMed: 17612631]
26. Nall BT, Zuniga EH, White TB, Wood LC, Ramdas L. Replacement of a conserved proline and the alkaline conformational change in *iso*-2-cytochrome-*c*. Biochemistry. 1989; 28:9834–9839. [PubMed: 2558730]
27. Garcia-Heredia JM, Diaz-Moreno I, Nieto PM, Orzaez M, Kocanis S, Teixeira M, Perez-Paya E, Diaz-Quintana A, De la Rosa MA. Nitration of tyrosine 74 prevents human cytochrome *c* to play a key role in apoptosis signaling by blocking caspase-9 activation. Biochim Biophys Acta Bioenerg. 2010; 1797:981–993.
28. Josephs TM, Liptak MD, Hughes G, Lo A, Smith RM, Wilbanks SM, Bren KL, Ledgerwood EC. Conformational change and human cytochrome *c* function: mutation of residue 41 modulates caspase activation and destabilizes Met-80 coordination. J Biol Inorg Chem. 2013; 18:289–297. [PubMed: 23334161]
29. Koshy TI, Luntz TL, Schejter A, Margoliash E. Changing the invariant proline-30 of rat and *Drosophila melanogaster* cytochromes *c* to alanine or valine destabilizes the heme crevice more than the overall conformation. Proc Natl Acad of Sci USA. 1990; 87:8697–8701. [PubMed: 2174161]
30. Ying T, Wang ZH, Lin YW, Xie J, Tan X, Huang ZX. Tyrosine-67 in cytochrome *c* is a possible apoptotic trigger controlled by hydrogen bonds via a conformational transition. Chem Commun. 2009:4512–4514.
31. Gu J, Yang S, Rajic AJ, Kurnikov IV, Prytkova TR, Pletneva EV. Control of cytochrome *c* redox reactivity through off-pathway modifications in the protein hydrogen-bonding network. Chem Commun. 2014; 50:5355–5357.
32. Alvarez-Paggi D, Castro MA, Tórtora V, Castro L, Radi R, Murgida DH. Electrostatically driven second-sphere ligand switch between high and low reorganization energy forms of native cytochrome *c*. J Am Chem Soc. 2013; 135:4389–4397. [PubMed: 23458571]

33. Harpaz Y, Gerstein M, Chothia C. Volume changes on protein folding. Structure. 1994; 2:641–649. [PubMed: 7922041]
34. Tognaccini L, Ciaccio C, D'Oria V, Cervelli M, Howes BD, Coletta M, Mariottini P, Smulevich G, Fiorucci L. Structure-function relationships in human cytochrome *c*: The role of tyrosine 67. J Inorg Biochem. 2016; 155:56–66. [PubMed: 26610191]
35. Patel CN, Lind MC, Pielak GJ. Characterization of horse cytochrome *c* expressed in *Escherichia coli*. Protein Expr Purif. 2001; 22:220–224. [PubMed: 11437597]
36. Berry EA, Trumpower BL. Simultaneous determination of hemes-*a*, hemes-*b*, and hemes-*c* from pyridine hemochrome spectra. Anal Biochem. 1987; 161:1–15. [PubMed: 3578775]
37. Inubushi T, Becker ED. Efficient detection of paramagnetically shifted NMR resonances by optimizing the WEFT pulse sequence. J Magn Reson. 1983; 51:128–133.
38. Zhong F, Lisi GP, Collins DP, Dawson JH, Pletneva EV. Redox-dependent stability, protonation, and reactivity of cysteine-bound heme proteins. Proc Natl Acad of Sci USA. 2014; 111:E306–E315. [PubMed: 24398520]
39. Nozaki Y. The preparation of guanidine hydrochloride. Meth Enzymol. 1972; 26:43–50. [PubMed: 4680720]
40. Creighton, TF. Protein structure: a practical approach. Oxford University Press; New York: p. 1997
41. Galo AL, Colombo MF. Singular value decomposition and ligand binding analysis. J Spectr. 2013; 2013:7.
42. Hendler RW, Shrager RI. Deconvolutions based on singular value decomposition and the pseudoinverse: a guide for beginners. Journal of Biochemical and Biophysical Methods. 1994; 28:1–33. [PubMed: 8151067]
43. Viola F, Aime S, Coletta M, Desideri A, Fasano M, Paoletti S, Tarricone C, Ascenzi P. Azide, cyanide, fluoride, imidazole and pyridine binding to ferric and ferrous native horse heart cytochrome *c* and to its carboxymethylated derivative: A comparative study. J Inorg Biochem. 1996; 62:213–222. [PubMed: 8627283]
44. Sutin N, Yandell JK. Mechanisms of the reactions of cytochrome *c*. J Biol Chem. 1972; 247:6932–6936. [PubMed: 4343163]
45. Ferrer JC, Guillemette JG, Bogumil R, Inglis SC, Smith M, Mauk AG. Identification of Lys79 as an iron ligand in one form of alkaline yeast *iso*-1-ferricytochrome *c*. J Am Chem Soc. 1993; 115:7505–7508.
46. Ubbink M, Campos AP, Teixeira M, Hunt NI, Hill HA, Canters GW. Characterization of mutant Met100Lys of cytochrome *c*-550 from *Thiobacillus versutus* with lysine-histidine heme ligation. Biochemistry. 1994; 33:10051–10059. [PubMed: 8060974]
47. Moore GR, Williams RJP. The solution structures of tuna and horse cytochromes *c*. Eur J Biochem. 1980; 103:533–541. [PubMed: 6244162]
48. Wang Z, Ando Y, Nugraheni AD, Ren C, Nagaoa S, Hirota S. Self-oxidation of cytochrome *c* at methionine80 with molecular oxygen induced by cleavage of the Met–heme iron bond. Mol BioSyst. 2014; 10:3130–3137. [PubMed: 25224641]
49. Myer Y, Kumar S, Kinnally K, Pande J. Methionine-oxidized horse heart cytochromes *c*. II. Conformation and heme configuration. J Protein Chem. 1987; 6:321–342.
50. Bren KL, Gray HB. Structurally engineered cytochromes with novel ligand-binding sites: Oxy and carbon monoxy derivatives of semisynthetic horse heart Ala80 cytochrome *c*. J Am Chem Soc. 1993; 115:10382–10383.
51. Lu Y, Casimiro DR, Bren KL, Richards JH, Gray HB. Structurally engineered cytochromes with novel ligand-binding properties. Expression of *S. cerevisiae* Met80Ala iso-1-cytochrome *c*. Proc Natl Acad Sci USA. 1993; 90:11456–11459. [PubMed: 8265573]
52. Wallace CJ, Clark-Lewis I. Functional role of heme ligation in cytochrome *c*. Effects of replacement of methionine 80 with natural and non-natural residues by semisynthesis. J Biol Chem. 1992; 267:3852–3861. [PubMed: 1310985]
53. Banci L, Bertini I, Bren KL, Gray HB, Turano P. pH-dependent equilibria of yeast Met80Ala-iso-1-cytochrome *c* probed by NMR spectroscopy: a comparison with the wild-type protein. Chem Biol. 1995; 2:377–383. [PubMed: 9383439]

54. Scott, RA., Mauk, AG., editors. Cytochrome c – A Multidisciplinary Approach. University Science Books; Sausalito, CA: 1996.
55. Eddowes MJ, Hill HAO. Electrochemistry of horse heart cytochrome-*C*. J Am Chem Soc. 1979; 101:4461–4464.
56. Barker PD, Mauk AG. pH-Linked conformational regulation of a metalloprotein oxidation-reduction equilibrium: electrochemical analysis of the alkaline form of cytochrome *c*. J Am Chem Soc. 1992; 114:3619–3624.
57. Sedlak E. Characterization of the polyanion-induced molten globule-like state of cytochrome c. Biopolymers. 2007; 86:119–126. [PubMed: 17330862]
58. Silkstone GG, Cooper CE, Svistunenko D, Wilson MT. EPR and optical spectroscopic studies of Met80X mutants of yeast ferricytochrome *c*. Models for intermediates in the alkaline transition. J Am Chem Soc. 2005; 127:92–99. [PubMed: 15631458]
59. Marques HM. Insights into porphyrin chemistry provided by the microperoxidases, the haempeptides derived from cytochrome *c*. Dalton Trans. 2007:4371–4385. [PubMed: 17909648]
60. Jordan T, Eads JC, Spiro TG. Secondary and tertiary structure of the A-state of cytochrome c from resonance Raman spectroscopy. Prot Sci. 1995; 4:716–728.
61. Davies AM, Guillemette JG, Smith M, Greenwood C, Thurgood AG, Mauk AG, Moore GR. Redesign of the interior hydrophilic region of mitochondrial cytochrome *c* by site-directed mutagenesis. Biochemistry. 1993; 32:5431–5435. [PubMed: 8388720]
62. Dyson HJ, Beattie JK. Spin state and unfolding equilibria of ferricytochrome *c* in acidic solutions. J Biol Chem. 1982; 257:2267–2273. [PubMed: 6277891]
63. Lett CM, Guillemette JG. Increasing the redox potential of isoform 1 of yeast cytochrome *c* through the modification of select haem interactions. BIochem J. 2002; 362:281–287. [PubMed: 11853535]
64. Lan WX, Wang ZH, Yang ZZ, Ying TL, Zhang X, Tan XS, Liu ML, Cao CY, Huang ZX. Structural basis for cytochrome *c* Y67H mutant to function as a peroxidase. Plos One. 2014; 9
65. Luntz TL, Schejter A, Garber EAE, Margoliash E. Structural significance of an internal water molecule studied by site-directed mutagenesis of tyrosine-67 in rat cytochrome *c*. Proc Natl Acad of Sci USA. 1989; 86:3524–3528. [PubMed: 2542935]
66. Redzic JS, Bowler BE. Role of hydrogen bond networks and dynamics in positive and negative cooperative stabilization of a protein. Biochemistry. 2005; 44:2900–2908. [PubMed: 15723532]
67. Lett CM, Berghuis AM, Frey HE, Lepock JR, Guillemette JG. The role of a conserved water molecule in the redox-dependent thermal stability of *iso*-1-cytochrome *c*. J Biol Chem. 1996; 271:29088–29093. [PubMed: 8910563]
68. Berghuis AM, Guillemette JG, Smith M, Brayer GD. Mutation of tyrosine-67 to phenylalanine in cytochrome *c* significantly alters the local heme environment. J Mol Biol. 1994; 235:1326–1341. [PubMed: 8308895]
69. Saigo S. Kinetic and equilibrium studies of alkaline isomerization of vertebrate cytochromes-*C*. Biochim Biophys Acta. 1981; 669:13–20. [PubMed: 6271238]
70. Wallace CJA, Mascagni P, Chait BT, Collawn JF, Paterson Y, Proudfoot AEI, Kent SBH. Substitutions engineered by chemical synthesis at 3 conserved sites in mitochondrial cytochrome-*C* – thermodynamic and functional consequences. J Biol Chem. 1989; 264:15199–15209. [PubMed: 2475497]
71. Schejter A, Koshy TI, Luntz TL, Sanishvili R, Vig I, Margoliash E. Effects of mutating Asn-52 to isoleucine on the heme-linked properties of cytochrome-*C*. Biochem J. 1994; 302:95–101. [PubMed: 8068029]
72. Pollock WBR, Rosell FI, Twitchett MB, Dumont ME, Mauk AG. Bacterial expression of a mitochondrial cytochrome *c*. Trimethylation of Lys72 in yeast *iso*-1-cytochrome *c* and the alkaline conformational transition. Biochemistry. 1998; 37:6124–6131. [PubMed: 9558351]
73. Baddam S, Bowler BE. Mutation of asparagine 52 to glycine promotes the alkaline form of *iso*-1-cytochrome *c* and causes loss of cooperativity in acid unfolding. Biochemistry. 2006; 45:4611–4619. [PubMed: 16584196]
74. McClelland LJ, Bowler BE. Lower protein stability does not necessarily increase local dynamics. Biochemistry. 2016; 55:2681–2693. [PubMed: 27104373]

75. Rosell FI, Harris TR, Hildebrand DP, Dopner S, Hildebrandt P, Mauk AG. Characterization of an alkaline transition intermediate stabilized in the Phe82Trp variant of yeast *iso*-1-cytochrome *c*. Biochemistry. 2000; 39:9047–9054. [PubMed: 10913318]
76. Ying TL, Zhong FF, Xie J, Feng YJ, Wang ZH, Huang ZX, Tan XS. Evolutionary alkaline transition in human cytochrome *c*. J Bioenerg Biomemb. 2009; 41:251–257.
77. Goldes ME, Jeakins-Cooley ME, McClelland LJ, Mou TC, Bowler BE. Disruption of a hydrogen bond network in human versus spider monkey cytochrome *c* affects heme crevice stability. J Inorg Biochem. 2016; 158:62–69. [PubMed: 26775610]
78. Garcia-Heredia JM, Diaz-Quintana A, Salzano M, Orzaez M, Perez-Paya E, Teixeira M, De la Rosa MA, Diaz-Moreno I. Tyrosine phosphorylation turns alkaline transition into a biologically relevant process and makes human cytochrome *c* behave as an anti-apoptotic switch. J Biol Inorg Chem. 2011; 16:1155–1168. [PubMed: 21706253]
79. Caffrey MS, Cusanovich MA. Site-specific mutagenesis studies of cytochromes-*C*. Biochim Biophys Acta Bioenerg. 1994; 1187:277–288.
80. Feinberg BA, Petro L, Hock G, Qin WY, Margoliash E. Using entropies of reaction to predict changes in protein stability: tyrosine-67-phenylalanine variants of rat cytochrome *c* and yeast *iso*-1 cytochromes *c*. J Pharmaceut Biomed. 1999; 19:115–125.
81. Maity H, Maity M, Englander SW. How cytochrome *c* folds, and why: submolecular foldon units and their stepwise sequential stabilization. J Mol Biol. 2004; 343:223–233. [PubMed: 15381432]
82. Hartshorn RT, Moore GR. A denaturation-induced proton-uptake study of horse ferricytochrome *c*. Biochem J. 1989; 258:599–605. [PubMed: 2539813]
83. Tonge P, Moore GR, Wharton CW. Fourier-transform infra-red studies of the alkaline isomerization of mitochondrial cytochrome *c* and the ionization of carboxylic acids. Biochem J. 1989; 258:599–605. [PubMed: 2539813]
84. Isom DG, Castañeda CA, Cannon BR, Velu PD, García-Moreno EB. Charges in the hydrophobic interior of proteins. Proc Natl Acad of Sci USA. 2010; 107:16096–16100. [PubMed: 20798341]
85. McClelland LJ, Mou TC, Jeakins-Cooley ME, Sprang SR, Bowler BE. Structure of a mitochondrial cytochrome *c* conformer competent for peroxidase activity. Proc Natl Acad of Sci USA. 2014; 111:6648–6653. [PubMed: 24760830]
86. Yao Y, Qian C, Ye K, Wang J, Bai Z, Tang W. Solution structure of cyanoferricytochrome *c*: ligand-controlled conformational flexibility and electronic structure of the heme moiety. J Biol Inorg Chem. 2002; 7:539–547. [PubMed: 11941512]
87. Galinato MG, Kleingardner JG, Bowman SE, Alp EE, Zhao J, Bren KL, Lehnert N. Heme-protein vibrational couplings in cytochrome *c* provide a dynamic link that connects the heme-iron and the protein surface. Proc Natl Acad Sci USA. 2012; 109:8896–8900. [PubMed: 22619327]
88. Volkov AN, Nicholls P, A WJ. The complex of cytochrome *c* and cytochrome *c* peroxidase: the end of the road? Biochim Biophys Acta. 2011; 1807:1482–1503. [PubMed: 21820401]
89. Lange C, Hunte C. Crystal structure of the yeast cytochrome bc_1 complex with its bound substrate cytochrome c. Proc Natl Acad Sci USA. 2002; 99:2800–2805. [PubMed: 11880631]
90. Maneg O, Malatesta F, Ludwig B, Drosou V. Interaction of cytochrome *c* with cytochrome oxidase: two different docking scenarios. Biochim Biophys Acta. 2004; 1655:274–281. [PubMed: 15100042]
91. Bertini I, Chevance S, Del Conte R, Lalli D, Turano P. The anti-apoptotic Bcl-xL protein, a new piece in the puzzle of cytochrome *c* interactome. PLoS ONE. 2011; 6:e18329. [PubMed: 21533126]
92. Diederix REM, Ubbink M, Canters GW. The peroxidase activity of cytochrome *c*-550 from *Paracoccus versutus*. Eur J Biochem. 2001; 268:4207–4216. [PubMed: 11488914]
93. Morison IM, Cramer Bordé EM, Cheesman EJ, Cheong PL, Holyoake AJ, Fichelson S, Weeks RJ, Lo A, Davies SMK, Wilbanks SM, Fagerlund RD, Ludgate MW, da Silva Tatley FM, Coker MSA, Bockett NA, Hughes G, Pippig DA, Smith MP, Capron C, Ledgerwood EC. A mutation of human cytochrome *c* enhances the intrinsic apoptotic pathway but causes only thrombocytopenia. Nat Genetics. 2008; 40:387–389. [PubMed: 18345000]
94. De Rocco D, Cerqua C, Goffrini P, Russo G, Pastore A, Meloni F, Nicchia E, Moraes CT, Pecci A, Salviati L, Savoia A. Mutations of cytochrome *c* identified in patients with thrombocytopenia

THC4 affect both apoptosis and cellular bioenergetics. Biochim Biophys Acta. 2014; 1842:269–274. [PubMed: 24326104]

95. Karsisiotis AI, Deacon OM, Wilson MT, Macdonald C, Blumenschein TM, Moore GR, Worrall JA. Increased dynamics in the 40–57 Omega-loop of the G41S variant of human cytochrome *c* promote its pro-apoptotic conformation. Sci Rep. 2016; 6:30447. [PubMed: 27461282]
96. Liptak MD, Fagerlund RD, Ledgerwood EC, Wilbanks SM, Bren KL. The proapoptotic G41S mutation to human cytochrome *c* alters the heme electronic structure and increases the electron self-exchange rate. J Am Chem Soc. 2011; 133:1153–1155. [PubMed: 21192676]

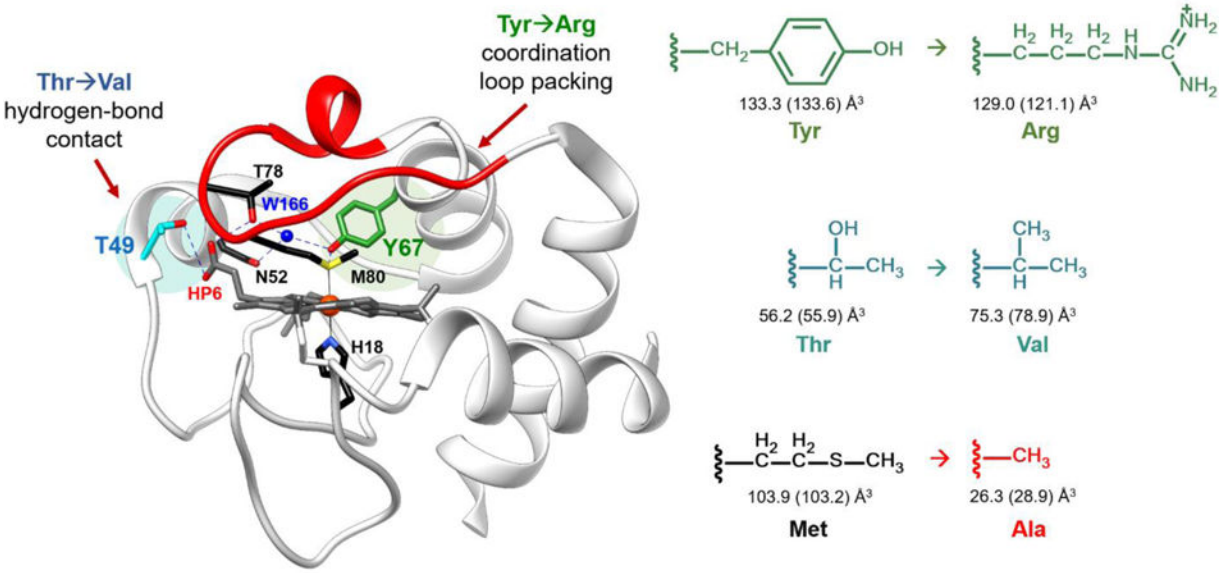

Figure 1.

Structure of WT horse heart cyt *c* (PDB ID: 1HRC).[6] Highlighted are the residues participating in the intraprotein hydrogen-bonding networks. A hydrogen-bond contact between the hydroxyl of Thr49 (*cyan*) and carboxyl group of outer-heme priopionate-6 was broken by mutating the residue to Val. Coordination loop packing was perturbed by mutating Tyr67 (*green*) to Arg, which also participates in the hydrogen-bonding network between Met80 and Thr78. Shown in right are the corresponding side chains of the amino acids introduced in the variants studied, with the side chain volumes (SC_{vol}) of the amino acids shown when buried and in solution (in parentheses); $SC_{vol} = V_{aa} - V_{gly}$.[33]

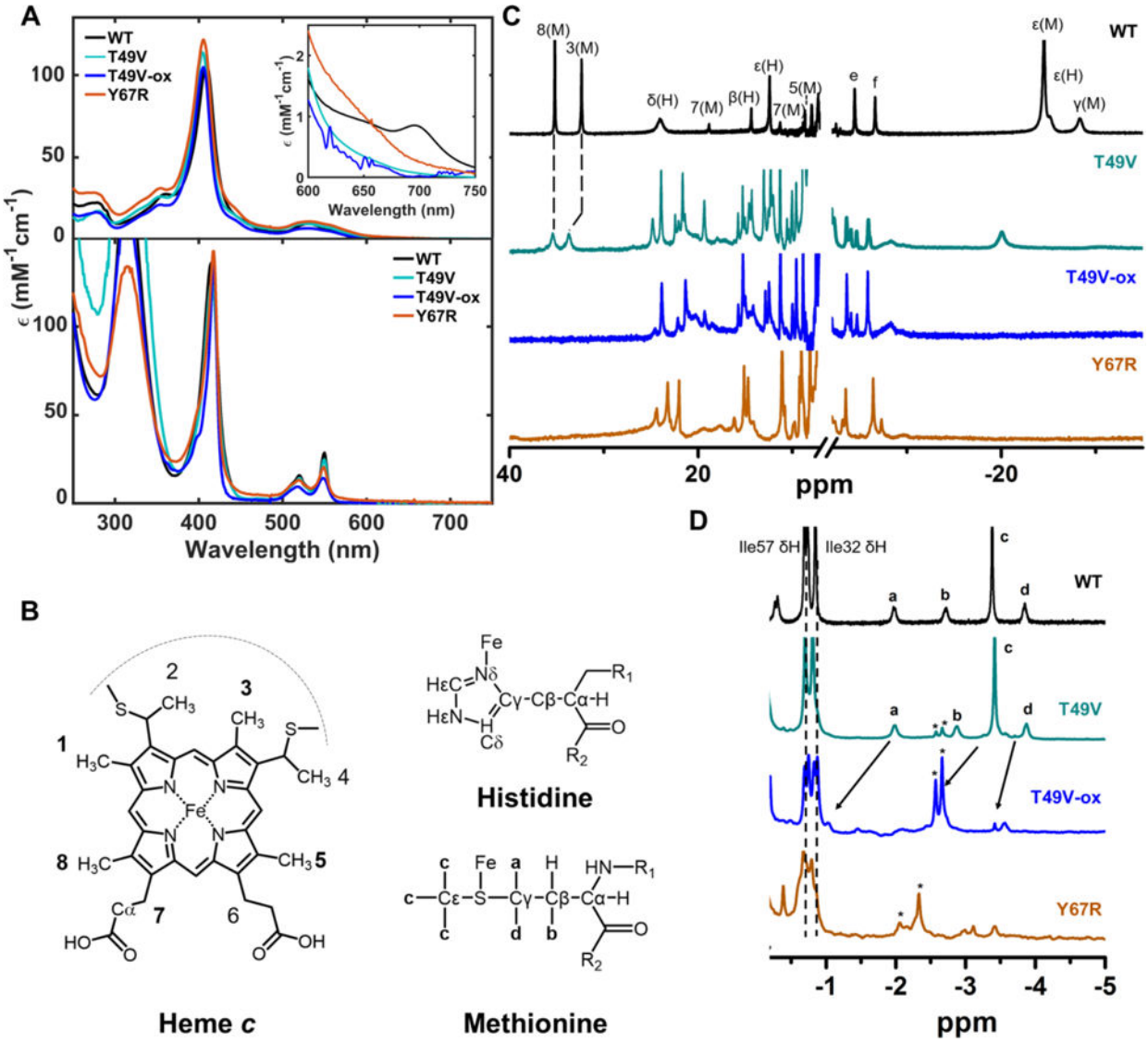

Figure 2.

Spectra of WT (*black*), T49V (*cyan*), T49V-MetSO (*blue*), and Y67R (*orange*) horse heart cyt *c* at pH (or pD) 7.4. (A) Absorption spectra of ferric (*top*) and ferrous (*bottom*) proteins at 22 ± 2 °C. (B) Structures of heme, His and Met showing the labeling nomenclature. (C) ^{1}H NMR spectra of ferric proteins and (D) ^{1}H NMR spectra of ferrous proteins at 25 °C. Numbered peaks correspond to protons in the heme porphyrin, with the identity of the iron ligand in parenthesis. Other labels correspond to M= Met80 or H= His18, e = Gly29 αH, and f= Pro30 δH. Peaks labeled with asterisk are the proton peaks of Met-SO.

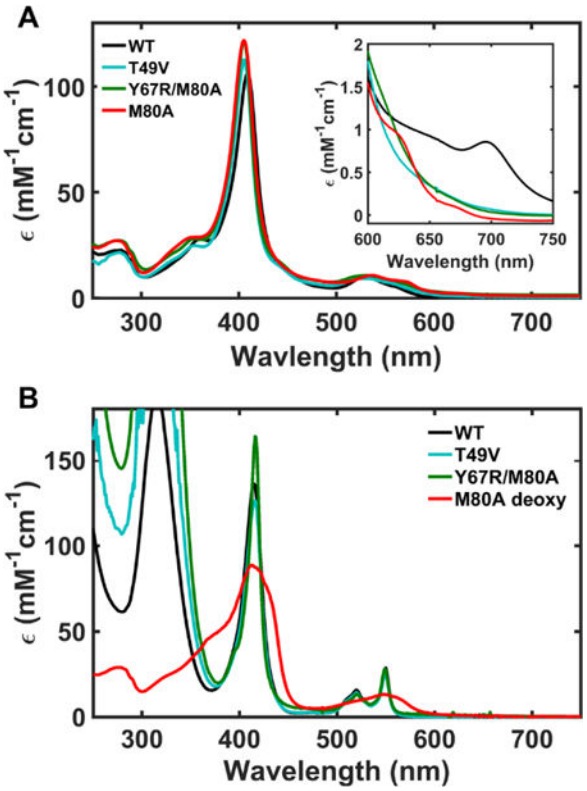

Figure 3.

Electronic absorption spectra of (A) ferric and (B) ferrous WT (*black*), T49V (*cyan*), Y67R/M80A (*green*), and M80A (*red*) at pH 7.4 and 22 ± 2 °C.

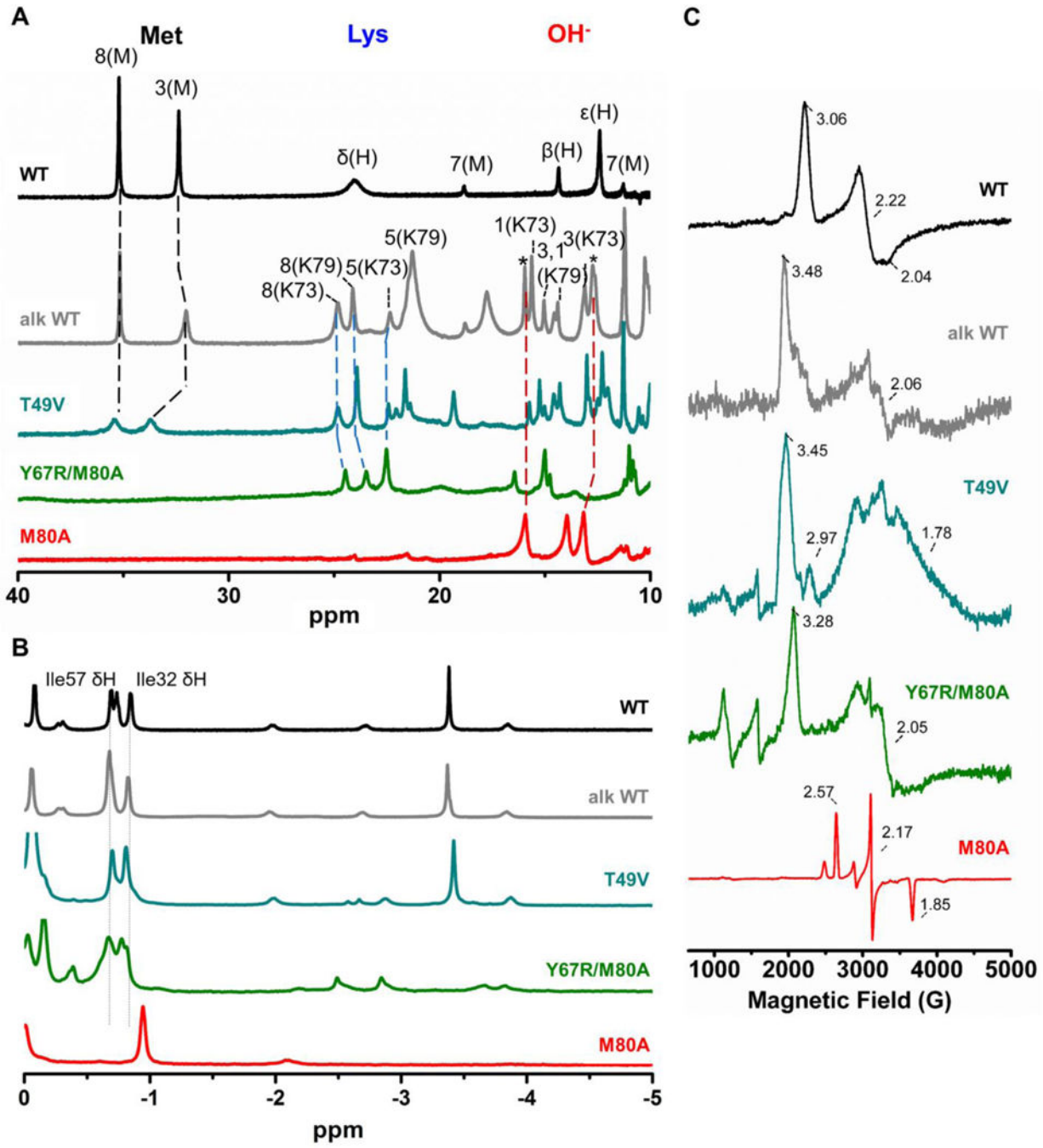

Figure 4.

^{1}H NMR spectra at 25 °C and EPR spectra at 10 K of WT (*black*), T49V (*cyan*), Y67R/M80A (*green*), and M80A (*red*) at pH (or pD) 7.4. ^{1}H NMR of (A) ferric and (B) ferrous proteins, with numbered peaks corresponding to protons in the heme porphyrin, with the identity of the ligand in parenthesis. Other labels correspond to M= Met80 or H= His18, e = Gly29 αH, and f= Pro30 δH (see Figure 2B for numbering). Spectra of alkaline WT (grey, pD 10.5)[14] are shown for comparison. (C) EPR spectra. Figure S2C displays pH-dependent changes in the EPR spectrum of M80A.

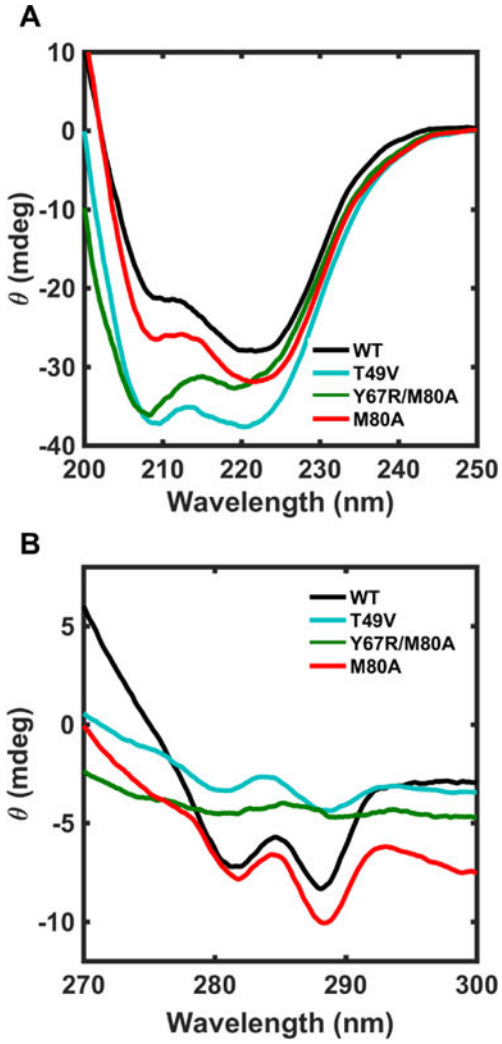

Figure 5.

(A) Far-UV ([cyt *c*]= 20 μM and *l*=1 mm) and (B) near-UV ([cyt *c*]= 200 μM and *l*=2 mm) CD spectra of WT (*black*), T49V (*cyan*), Y67R/M80A (*green*), and M80A (*red*) in a 100 mM sodium phosphate buffer at pH 7.4 and 22 ± 2 °C.

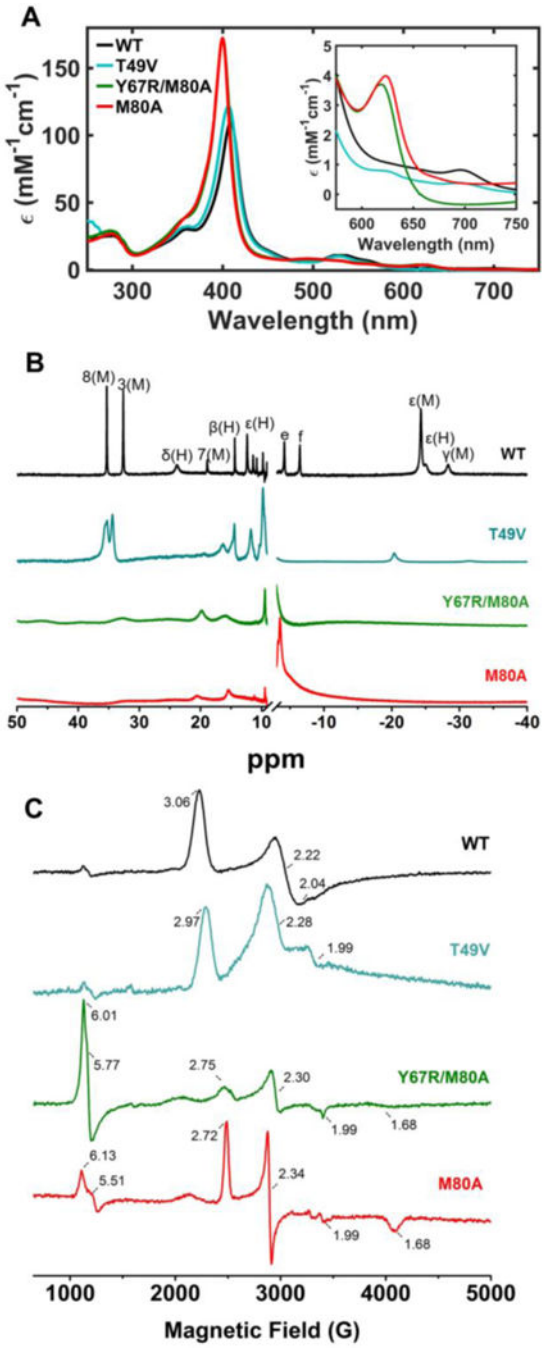

Figure 6.

(A) Electronic absorption spectra at 22 ± 2 °C, (B) ^{1}H NMR spectra at 25 °C, and (C) EPR spectra at 10 K of ferric WT (*black*), T49V (*cyan*), Y67R/M80A (*green*), and M80A (*red*) at pH (or pD) 4.5.

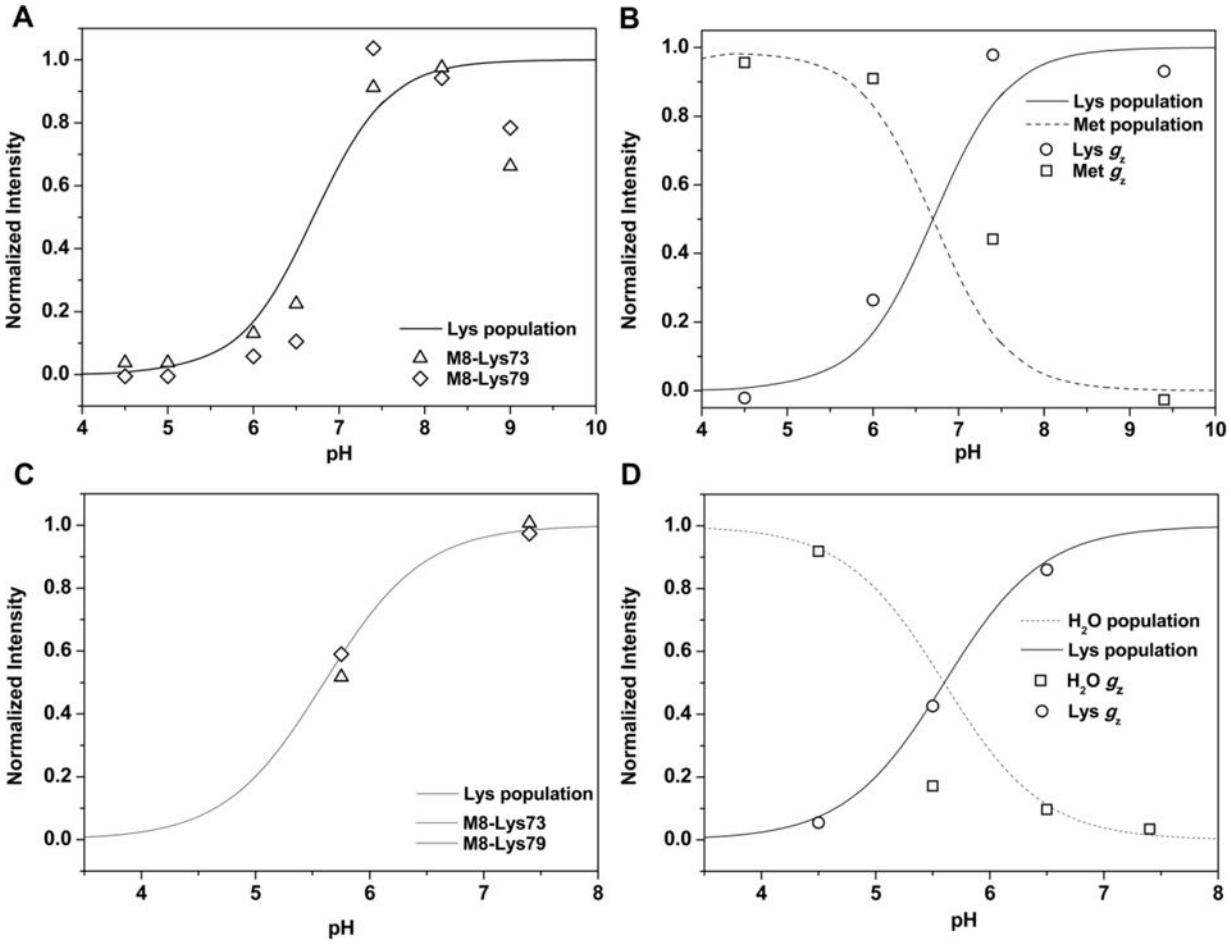

Figure 7.

pH dependence of the intensities of selected signals from (A) NMR and (B) EPR spectra of ferric T49V and (C) NMR and (D) EPR spectra of ferric Y67R/M80A. Solid lines are the populations of the Lys-ligated forms (T49 V and Y67R/M80A) and dashed lines are the populations of the Met-ligated form (T49V) and the H_2O-ligated form of (Y67R/M80A) as functions of pH.

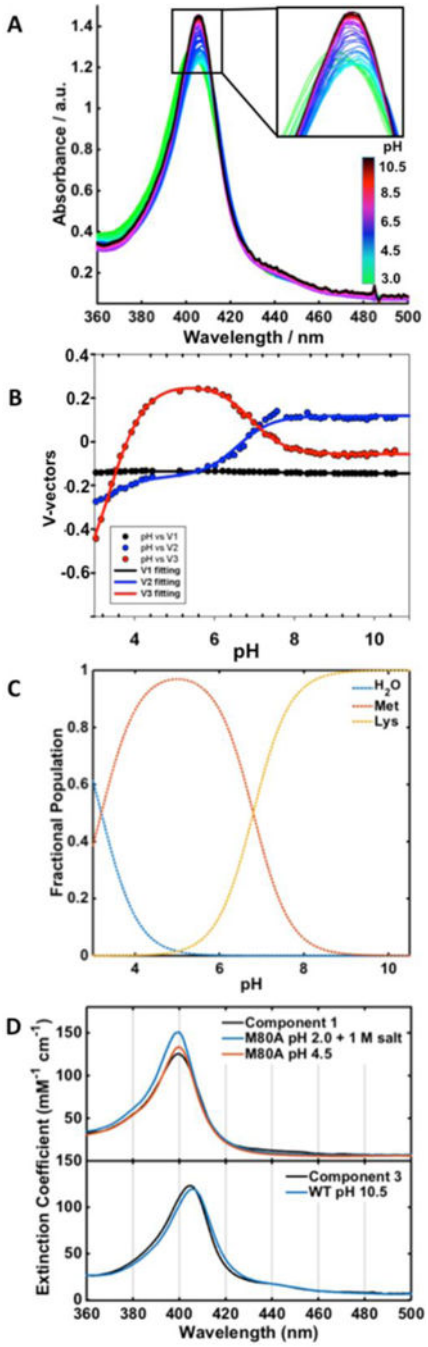

Figure 8.

(A) Electronic absorption spectra of T49V over a pH range from 3.0 to 10.5 at 22 ± 2 °C. (B) Plots of the V-vectors from SVD analysis of these spectra. (C) Fractional populations F_i of the three components using pK_{a1} = 3.3 and pK_{a2} = 6.8. (D) Spectra of Components 1 and 3 from SVD analysis are compared to that of H_2O-ligated M80A pH 2.0 with 1 M salt and at pH 4.5 (*top*) and Lys-ligated WT at pH 10.5 (*bottom*). The spectrum of Met-ligated WT at pH 7.4 was used as an input for Component 2.

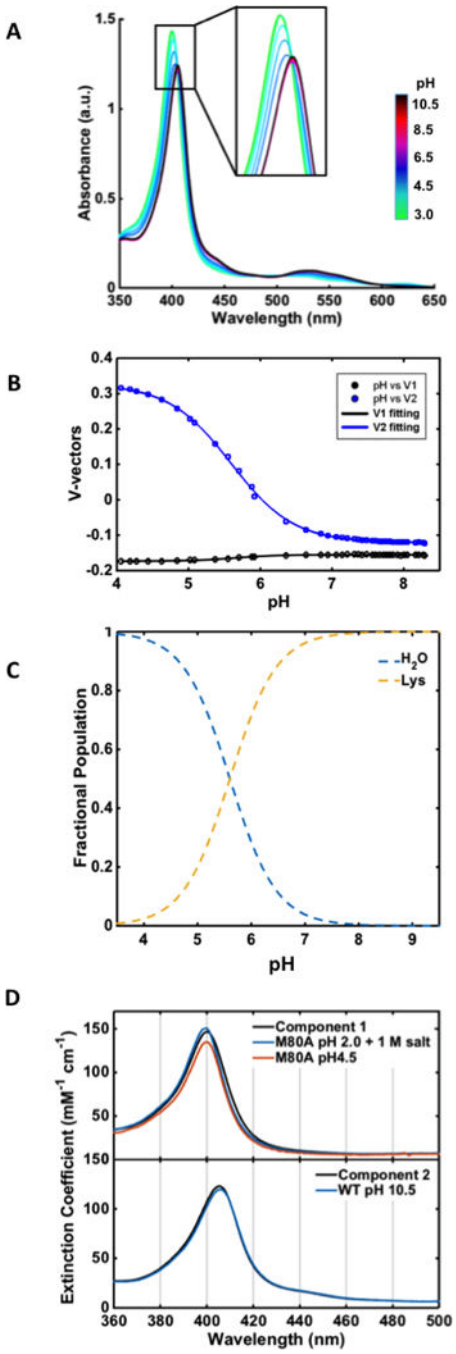

Figure 9.

(A) Electronic absorption spectra of Y67R/M80A over a pH range from 4.0 to 8.3 at 22 ± 2 °C. (B) Plots of the V-vectors from SVD analysis of these spectra. (C) Fractional populations F_i of the two components using pK_a = 5.6. (D) Spectra of the two components from SVD analysis are compared to that of H_2O-ligated M80A at pH 4.5 and at pH 2.0 with 1 M added salt (*top*) and Lys-ligated WT at pH 10.5 (*bottom*).

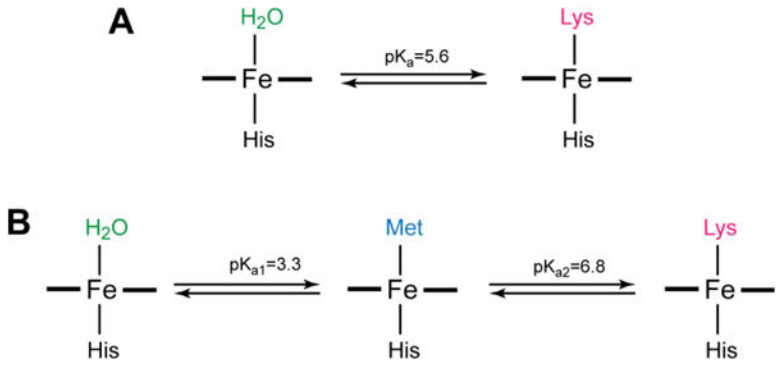

Figure 10.

Models for pH-dependent changes in ligation considered in the analyses of (A) Y67R/M80A and (B) T49V horse heart cyt *c* variants.

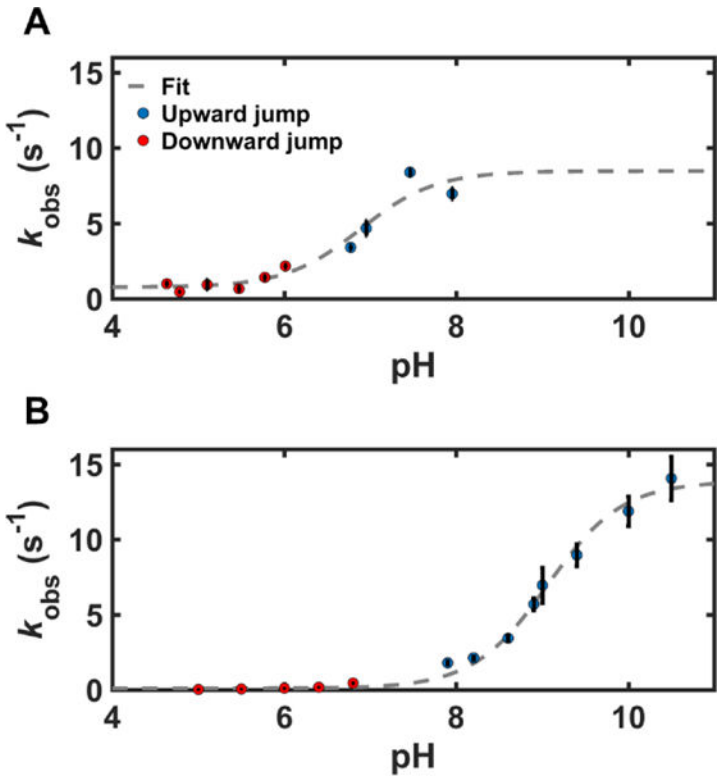

Figure 11.

Plots of k_{obs} versus pH, with fits (*gray*, dashed line) to eq 7 for (A) Y67R/M80A and (B) T49V. Results from downward (*red* circles) and upward (*blue* circles) pH-jump experiments at 22 ± 2 °C are shown.

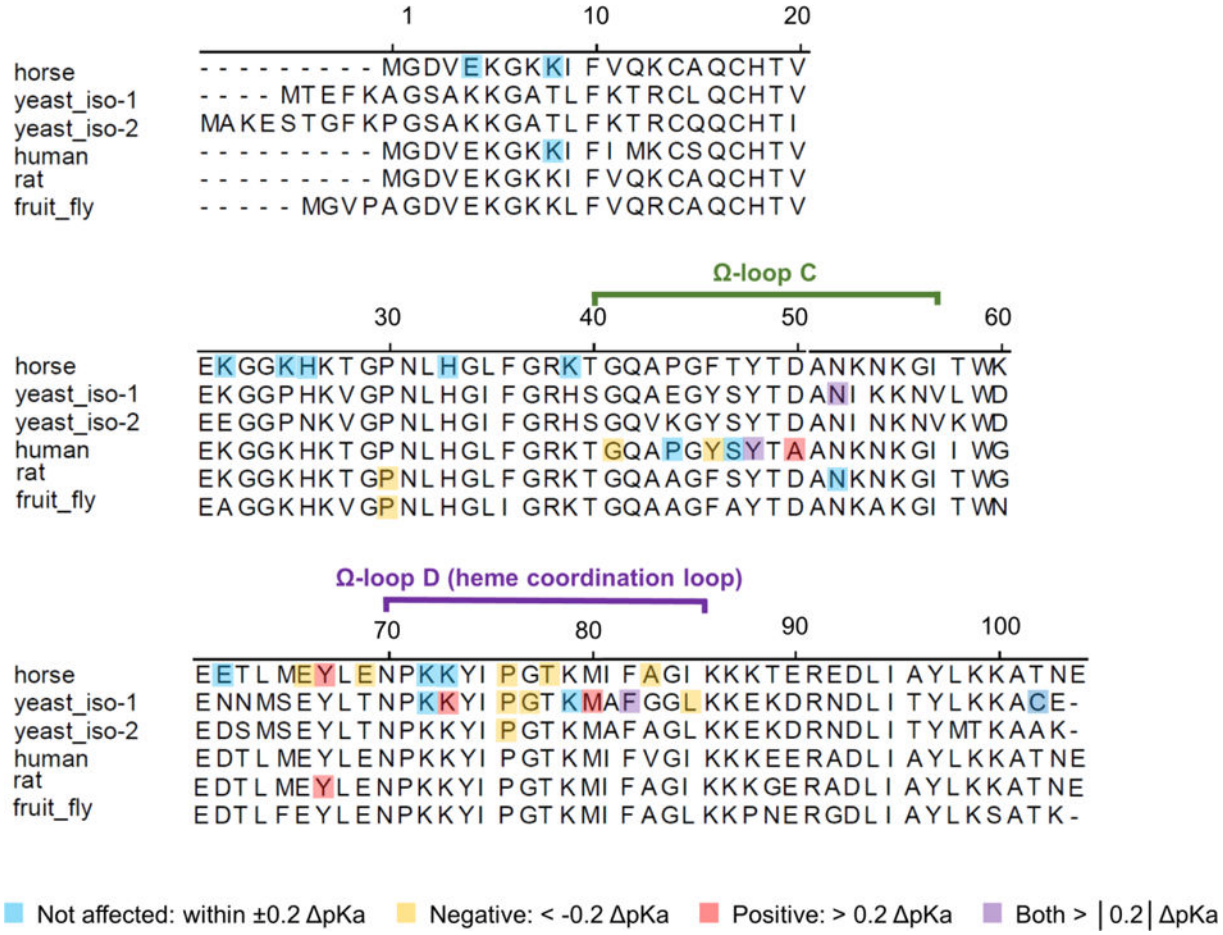

Figure 12.

Sequence alignment of cyt *c* from various species, for which information about mutational effects on the pK_a value for the alkaline transition is available. Highlighted are mutation sites, color-coded by the magnitude and direction of the change in the pK_a value. Table S1 lists the mutants and their pK_as.

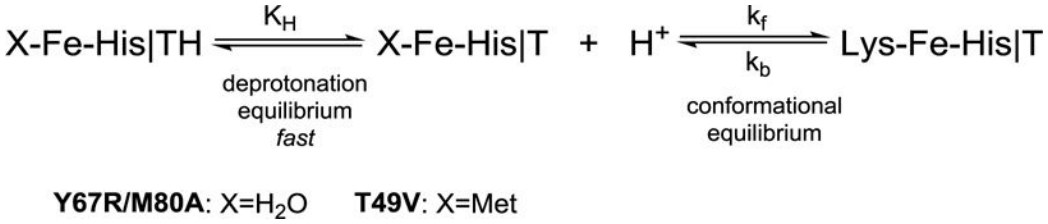

Scheme 1.

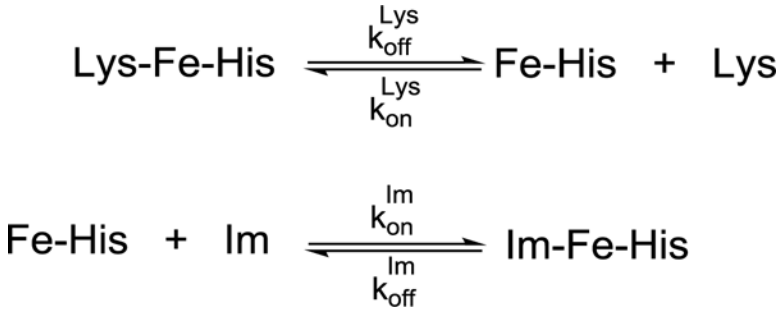

Scheme 2.

Table 1

Reduction Potentials of Horse Heart Cytochrome *c* Variants[a]

Variant	pH	Axial ligand	E° (mV vs SHE)
WT	7.8	Met	255[b]
	10.0	Lys	−205[c]
T49V	4.5	Met (major)	144 ± 5 (240 ± 5)[d]
		H_2O (minor)	
	7.4	Lys (major)	−15 ± 8 (−15 ± 8)
		Met (minor)	
Y67R/M80A	4.5	H_2O	−54 ± 7 (−22 ± 3)
	7.4	Lys	−80 ± 7 (−56 ± 1)
M80A	4.5	H_2O	16 ± 6 (32 ± 3)
	7.4	OH^-	−33 ± 4 (–)
	7.0		185[e]

[a] In this work, potentials were determined from spectroelectrochemistry experiments performed at 22 ± 2 °C.

[b] From ref. 55.

[c] From ref. 56.

[d] Reductive (oxidative) direction.

[e] From ref. 52.

Table 2

Thermodynamic Parameters for the Unfolding Transitions of Horse Heart Ferricytochrome *c* Variants[a]

Variant	pH	Thermal Denaturation		GuHCl-Induced Denaturation[b]		
		T_m (K)	ΔH_D (kJ mol^{-1})	$[GuHCl]_{1/2}$ (M)	m_D (kJ mol^{-1} M^{-1})	$-\Delta G_f$ (kJ mol^{-1})
WT	7.4	357.1[c]	360 ± 30[c]	2.7 ± 0.1[d]	11.5 ± 2.6[d]	31.1 ± 7.1[d]
	4.5	344 ± 1.0	205 ± 30	2.6 ± 0.1	9.8± 0.2	25.1 ± 0.7
T49V	7.4	359 ± 1.6	351 ± 130	2.7 ± 0.1	11.2 ± 3.7	30.2 ± 10.1
	4.5	345 ± 0.8	132 ± 87	2.5 ± 0.2	6.7 ± 1.9	16.7 ± 4.9
Y67R/M80A	7.4	344 ± 1.5	133 ± 4	1.7 ± 0.1	10.3 ± 0.1	17.5 ± 1.0
	4.5	328 ± 0.4	151 ± 1	1.4 ± 0.04	9.6 ± 1.3	13.4 ± 1.9
M80A	7.4	357 ± 0.7	306 ± 79	2.71 ± 0.02	10.3 ± 0.6	27.9 ± 1.6
	4.5	349 ± 1.1	344 ± 55	2.6 ± 0.1	11.6 ± 0.3	30.2 ± 1.4

[a] Monitored is ellipticity at 222 nm.

[b] Performed at 22 ± 2 °C.

[c] From differential scanning calorimetry, pH 7.0, ref. 57.

[d] From ref. 8.

Table 3

Parameters for pH-Dependent Transitions in Horse Heart Ferricytochrome *c*

	Ligand Exchange	Region Monitored	pK_a	n
WT[a]	His/H_2O → His/Met		2.5	1.14
	His/Met → His/Lys		9.35	1.0
T49V[b]	His/H_2O → His/Met	Soret	3.3 ± 0.1	1.0 ± 0.1
		CT	3.0 ± 0.1	0.9 ± 0.1
	His/Met → His/Lys	Soret	6.8 ± 0.1	1.0 ± 0.1
		CT	6.7 ± 0.1	1.0 ± 0.1
Y67R/M80A[b]	His/H_2O → His/Lys	Soret	5.6 ± 0.1	1.0 ± 0.1
		CT	5.6 ± 0.1	1.0 ± 0.1
M80A[b]	His/H_2O → His/OH^-	Soret	6.1 ± 0.1[c]	0.9 ± 0.1

[a] From ref. 13, performed at 20 °C.

[b] Performed at 22 ± 2 °C.

[c] A similar value has been reported in studies of semisynthetic M80A (ref. 50).

Table 4

Kinetic Parameters for the Alkaline Transition and Imidazole Binding for Horse Heart Ferricytochrome *c* Variants

Variant	k_f (s^{-1})	k_b (s^{-1})	K_C	pK_H	$pK_H + pK_c$	K_D^{Im} (M)	k_{obs}^{Im} (s^{-1})
WT	10.5 ± 0.2[a]	0.048[a]	218 ± 4[a]	11.5 ± 0.1[a]	9.2 ± 0.1	9.5×10^{-2}[b]	60 ±15
T49V[c]	13.7 ± 0.9	0.11 ± 0.02	125 ± 24	9.1 ± 0.1[d]	7.0 ± 0.1	1.4×10^{-3}	0.08 ± 0.01
Y67R/M80A[c]	7.7 ± 1.9	0.78 ± 0.38	9.9 ± 5.4	6.9 ± 0.4[d]	5.9 ± 0.5	2.9×10^{-4}	0.79 ± 0.05

[a] From ref. 75, performed at 25.0 ± 0.1 °C.

[b] Calculated from values in ref. 44.

[c] Performed at 22 ± 2 °C.

[d] Determined from the fit of the data in Figure 11.